Experimental Characterisation and Modelling of Polymer Foam Core Materials using the Virtual Fields Method and DIC

Wang, Peng

DOI (link to publication from Publisher):
10.5278/vbn.phd.engsci.00052

Publication date:
2015

Document Version
Publisher's PDF, also known as Version of record

EXPERIMENTAL CHARACTERISATION AND MODELLING OF POLYMER FOAM CORE MATERIALS USING THE VIRTUAL FIELDS METHOD AND DIC

BY
PENG WANG

DISSERTATION SUBMITTED 2015

AALBORG UNIVERSITY
DENMARK

Experimental Characterisation and Modelling of Polymer Foam Core Materials using the Virtual Fields Method and DIC

Ph.D. Thesis

by

Peng Wang

Department of Mechanical and Manufacturing Engineering

Aalborg University

Fibigerstræde 16,DK- 9220 Aalborg East

Denmark

Thesis submitted: December 3, 2015

PhD supervisor: Professor Ole Thybo Thomsen
Aalborg University

PhD committee: Associate Professor Esben Lindgaard (chairman)
Aalborg University, Denmark

Professor Michael Sutton
University of South Carolina; USA

Professor Michel Grédiac
Campus de Clermont-Ferrand, France

PhD Series: Faculty of Engineering and Science, Aalborg University

ISSN (online): 2246-1248
ISBN (online): 978-87-7112-423-1

Published by:
Aalborg University Press
Skjernvej 4A, 2nd floor
DK – 9220 Aalborg Ø
Phone: +45 99407140
aauf@forlag.aau.dk
forlag.aau.dk

Printed in Denmark by Rosendahls, 2015

Preface

This thesis is submitted as partial fulfilment of the requirements for the PhD degree. The work has been carried out during the period from September 2010 to December 2014 at the Department of Mechanical and Manufacturing Engineering, Aalborg University, Denmark.

The Project was co-sponsored by Innovation Fund Denmark (previously the Danish National Advanced Technology Foundation) through the project "Advanced Thermal Breaker", which has been carried out in close collaboration between the Department of Mechanical and Manufacturing Engineering, Aalborg University, Denmark and Fiberline Composites A/S, Middelfart, Denmark. The financial support is gratefully acknowledged.

The project has been supervised by Professor Ole Thybo Thomsen at the Department of Mechanical and Manufacturing Engineering, Aalborg University, Denmark and Professor Fabrice Pierron at Faculty of Engineering and the Environment, University of Southampton, UK. I am deeply grateful for the many discussions and their invaluable suggestions and encouragement through the project.

I also would like to acknowledge the colleagues at Aalborg University and employees in Fiberline Composite A/S for their kind help and support.

Finally, I would like to thank my family, especially my wife Shan for their love and support.

October 2015

Peng Wang

Abstract

Fiberline Composites A/S, a leading manufacturer of composite window profiles, is developing a new concept for window frames. Identifying suitable material systems is a particular challenge to develop the future high-performance window frames. Compared with the materials used for existing standard window frames, Fiberline Composites A/S aims to develop a new type of foam core material that will be placed inside the pultruded composite laminate profile to provide thermal insulation as well as structural support for the thin walled composite profile. Ideally, polymer foam core materials can be considered as homogenous isotropic materials. However, in practice most polymer foams display both heterogeneous and anisotropic material behaviour due to the density variations and directionality of foam cells developed during the manufacturing process. Following normal practices for mechanical testing of polymer foams it is necessary to conduct a large number of tests to derive average values of material constitutive parameters. The material properties obtained are often obscured by parasitic effects that are induced when conducting conventional tensile, shear and compressive tests, since these effects disturb the stress and strain fields thus making it very difficult to deduce the true material constitutive parameters.

This thesis presents an efficient and robust methodology to characterize the whole set of elastic constitutive stiffness parameters of polymer foam core materials using just in one single test. Two main experimental techniques were used: Digital Image Correlation (DIC) and the Virtual Fields Method (VFM). A modified Arcan fixture [1, 2] was used to provide complex multi-axial to the foam core samples. The loading angle and the off-axis angle of the principal material direction relative to the principal geometrical direction of the foam specimens are used as the two design variables. Noise and missing data effects are introduced as the two main error sources to construct a cost function to optimize the test configuration. After conducting an elaborate sensitivity study to identify the optimized test configurations, experimental validation was undertaken on both optimized and poorly setup test configurations. The results were compared with the reference parameters obtained using conventional uniaxial testing procedures.

Although the selected test configuration led to a notable improvement of the experimental results, significant differences were found between reference values of material parameters known from literature and/or other tests, and the experimental results from that study. It was thought that one of the reasons for this was that the conducted optimization study was based on finite element simulated strain fields which did not include the sources of error that arise from real DIC measurements. In particular, the low-pass spatial filtering effect of the DIC measurements will lead to underestimation of the strains in large strain gradients areas of the test specimen, which in turn will lead to biases on the identified stiffness components. Moreover, the low signal to noise ratio associated with the measurement of the elastic material

properties of polymer foams will tend to increase the random error (scatter) of the data. Accordingly, a prerequisite for resolving the issues identified from the previous study, and thereby providing more accurate and robust materials parameter identification, is the establishment of a reasonable quantification of the uncertainty of the measurements as well as further improvement of the experiments. It must be noted that establishing realistic uncertainty bounds in identified material parameters from such inverse approaches is key to the diffusion of such techniques to industry in the future. This topic has very rarely been approached in the past and when so, only the random error was addressed but not the bias arising from the spatial low-pass filtering effect mentioned above.

In order to solve the issues listed above, extensive work has been done in this PhD project to develop a more advanced procedure to realistically simulate the modified Arcan test for polymer foams using Digital Image Correlation and the Virtual Fields Method. The actual image recording process was mimicked by numerically generating a series of deformed synthetic images. Subsequent to this, the entire measurement and data processing procedure was simulated by processing the synthetic images using DIC and VFM algorithms. This procedure was used to estimate the uncertainty of the measurements (systematic and random errors) by including the most significant parameters of actual or physical experiments, e.g. the geometric test configuration, the parameters of the DIC process and the noise. By using these parameters as design variables, and by defining different error functions as object functions, an optimization study was performed to minimize the uncertainty of the material parameter identification and to select the optimal test parameters. The confidence intervals of the identified parameters were predicted based on systematic and random errors obtained from the simulations. The simulated experimental results have shown that averaging multiple images can lead to a significant reduction of the random error. Finally, an experimental determination of the elastic coefficient of a PVC foam material was conducted using the optimized test parameters obtained from the numerical study. The identified stiffness values matched well with data from previous tests, but even more interesting was the fact that the experimental uncertainty intervals matched reasonably well with the predictions of the simulations, which is a highly original result and an important outcome of this work.

List of contents

1. Introduction

1.1. Background and Motivation

Large amounts of energy are consumed for the heating of buildings. Roughly 30-60% of the energy loss of a building is due to windows and doors, hereof a significant part through the window frames that have higher thermal transmittance values than the glass. The political target is to reduce CO_2 emission by 75% in new buildings by 2020 in several European countries [1]. Therefore the market for high-performance window frames is very promising. Fiberline Composites A/S, a leading manufacturer of composite window profiles, is developing a new concept for window frames, which can provide super insulation and high strength with minimum cost of materials. For the development of this kind of window frames, Fiberline Composites A/S is exploring new material systems, including new types of polymer foam core materials to provide superior thermal insulation properties, and advanced thin-walled composite laminates made by pultrusion, to provide for the structural requirements. Therefore materials development and characterization (mechanical and thermal) are topics of primary importance for the development of material systems and the design of new window frames that are both energy and structurally effective.

This PhD project is part of a research project entitled "Advanced Thermal Breaker" co-funded by Innovation Fund Denmark, Fiberline Composites A/S and Aalborg University. The aim of project is to develop and take to market a new concept for composite/foam window frame systems that doubles the insulation capability as compared with existing window frame systems, and which at the same time fulfils the stiffness and strength requirements. To achieve this, extensive research needs to be carried out to be able to experimentally characterize and to model both the thermal barrier and the mechanical properties of these new material systems, so as to find the optimal combination of the two material systems (polymer foam and pultruded composites). Polymer foam materials are widely used as core materials in sandwich structures or as insulation materials (as is the case here), and they are ideally considered as homogenous isotropic materials [2]. However, in practice most polymer foams display both heterogeneous and anisotropic material behaviour due to the density variations and directionality of foam cells developed during the manufacturing process [3, 4]. Therefore accurate experimental characterization of the mechanical behaviour of polymeric foam materials is essential for their efficient use in sandwich structures, as well as for the development of accurate numerical models on the material and structural levels. Conventional mechanical test methods including tensile, shear or bending tests are widely used to characterize both

isotropic and orthotropic homogeneous materials. However there are significant difficulties associated with the application of such standard methods for the mechanical characterization of heterogeneous, anisotropic materials or functionally graded materials due to the presence of heterogeneous strain fields when the materials are subject to mechanical loading. In addition, it is normally required to conduct a large number of tests to deduce average values of material constitutive parameters, and parasitic effects occur during tensile, shear and compressive tests which can disturb the stress field [4, 5].

The overall goal of this PhD project is to develop a novel methodology for mechanical testing, which enables the extraction of all the elastic material parameters of polymer foam core materials (including manufacturing variations) from one single test. This methodology will be based on the Digital Image Correlation (DIC) technique combined with the Virtual Field Method. The design of the experimental methodology is optimized by introducing a new procedure to realistically simulate the whole measurement chain.

1.2 State of the art - Characterisation of polymer foam materials, Digital Image Correlation and the Virtual Fields Method

Cellular polymer closed cell foams are commonly used as core material in lightweight sandwich structures as well as for insulation purposes. Common polymer closed cell foams include Polyvinylchlorid (PVC), Polymethacrylimide (PMI), Polyurethane (PU) or polyethylene terephthalate (PET) foams. The orthotropic material behaviour of polymeric foams has been studied extensively in the literature [4-7]. Most of the studies rely on the use of several different testing methods including uniaxial tension, uniaxial compression and shear, conducted along with deformation measurements that are based on either point-wise or area-wise (averaged) measurement techniques like e.g. extensometers or strain gauges. Since Since polymer foam materials are relatively soft/compliant in comparison with most other engineering materials, the experimental measurement of the elastic material properties is very sensitive to stiffening and contact effects introduced by using conventional methods like e.g. strain gauges and clip gauges. For example, the adhesive used to bond strain gauges onto the foam surface may penetrate into the open foam cells thus reinforcing the core material locally, and this may lead to significant errors in the measured elastic coefficients. Also, clip gauges have a relatively large gauge length, and this makes it difficult to capture the foam deformation in critical areas in sufficient detail. Therefore, as an alternative, the use of a non-contact measurement technique would be beneficial in order to enable accurate mechanical characterization of polymer foam materials. Recent works [8] and [2] have addressed the characterization of the cross linked PVC foam material

Divinycell H100 [9] using Digital Image Correlation (DIC). Both of these studies measured the orthotropic properties of PVC foam, and the obtained results were in good agreement with the datasheets from the manufacturer [9]. However, the experimental design of these works was still based on the use of conventional mechanical testing methodology, necessitating the conduction of several tests. Essentially one test was conducted to obtain each elastic property/quantity to be measured, except for the Poisson's ratio that is extracted from a tensile test together with Young's modulus. A significant amount of time and effort was spent on designing the different test specimen shapes needed to reach a uniform stress/strain state in the gauge area.

Several of the listed drawbacks can potentially be overcome using full field measurement techniques such as Digital Image Correlation (DIC) [10-12], speckle pattern interferomerty [13] and grid methods [14-16]. These techniques can capture a heterogeneous strain field which involves the whole set of constitutive parameters, and it is conceivable to extract all the elastic coefficients from one single test. However no closed-form solution exists between such measurement(s) and the unknown material parameters sought for. To circumvent this problem different methodologies have been proposed to solve the inverse problem defined as the identification of a set of constitutive material parameters that minimizes the difference (expressed in terms of a residual) between the measured and a "calculated" field based on certain assumptions like e.g. elastic behaviour (or non-linear elastic, plastic or visco-elastic material behaviour), and where the "field" in principle can be displacements, strains or stresses. Among the "inverse" approaches can be mentioned the finite element model updating technique [17], the constitutive equation gap method [18], and the Virtual Fields Method (VFM) [19].

The VFM method is one of the most effective and popular techniques developed in recent years. This methodology is based on the principle of virtual work [20] to solve the inverse problem. In this case, integrals that involve/depend on the strain fields are included in the principle or governing field equations. These integrals can be approximated with the full-field measurements using e.g. DIC (or another full field measurement technique). The development of VFM and its applications is documented in [21, 22, 23]. The efficiency of this method is underlined by the fact that it does not require the use of iterative procedures to solve the inverse problem. Thus, the VFM approach is much less time consuming than e.g. classical finite element model updating approaches applied to similar applications [22, 23], and VFM used in conjunction with full-field deformation measurements is becoming widely used for the extraction of constitutive parameters for composites and other types of materials [20]. However, there have been relatively few studies concerning polymer foam materials using this technique, and the first attempt at identifying

Poisson's ratios of standard low-density (homogeneous) polyurethane foams by using DIC and VFM was only published recently [24].

One of the most important challenges to overcome when using such inverse procedures is to choose a suitable mechanical test configuration. Since the heterogeneous stress/strain fields play an important role in the identification procedure, it is very important to have a test configuration that activates all the sought constitutive parameters of the materials under investigation. This means that the actual stress/strain fields must be sufficiently sensitive to variations of each of the sought parameters. Optimization of the test configuration for VFM identification was firstly proposed in [25]. The idea was to identify an optimized specimen length and a material orthotropic axis angle so as to minimize a cost function based on the sensitivity to noise of the sought material stiffness components. Recently, a refined test configuration design procedure was proposed in [26]. The study used the grid method as the full-field technique and simulated the whole measurement and identification chain, including image forming and grid method algorithm. This study provided a significant improvement of the optimization procedure by introducing the many different types of error sources into the cost function. However, this approach was not fully validated experimentally. Moreover, it used a specific test fixture, namely the un-notched Iosipescu test as described in [25], and it is important to extend the optimization to other test configurations and full-field techniques, like DIC. Also more experimental work needs to be done to validate the optimization study.

1.3 Statement of objectives and outline of thesis

The present work aims to establish an efficient and reliable methodology to simultaneous identification of the orthotropic elastic stiffness components of a cross-linked PVC foam in one single mechanical test. This will be achieved by developing a robust optimization procedure to predict the uncertainty of the experimental characterisation of cross-linked PVC orthotropic foam materials and to optimize the design of the experiments. The structure and remaining chapters of this thesis are outlined as follow:

Chapter 2
Chapter 2 introduces the experimental setup developed and utilized throughout the project. The method is based on DIC to capture the heterogeneous strain field which involves the whole set of constitutive parameters in one single test. A Modified Arcan Fixture (MAF) is used to active the heterogeneous deformation field. The full deformation field is processed by the 'inverse' approach (The VFM method) described in Chapter 3 to extract full set of material parameters.

Chapter 3
Chapter 3 presents the basic idea of the Virtual Fields Method (VFM) and how to adopt the methodology to the experimental setup demonstrated in Chapter 2. The method is derived based on the principle of virtual work to process full-field measurements and solve the inverse problem directly.

Chapter 4
In Chapter 4, the methodology developed in Chapters 2 and 3 is applied on a PVC foam core material to validate the ability of the procedure to identify all the elastic parameters in actual test. The preliminary study reveals that the principal material parameter in the transverse material direction is very unstable and difficult to identify. The value of this parameter depends on different filtering techniques and the adopted smoothing level in the DIC procedure. Since the smoothing methodology is difficult to handle, the most feasible and efficient way to solve this problem is to modify the test configuration so that more transverse stresses/strains are introduced thus reducing the effect of noise. (Appended Paper 1).

Therefore, a numerical optimization study is performed with different loading angles of the MAF test fixture and different off-axis angles relative to the principal material axes. A finite element (FE) model is developed to simulate the strain fields with different test configurations. The objective is to identify the configuration that gives the minimum sensitivity to noise and missing data on the specimen edges, which are the two major issues when identifying the stiffness components from actual DIC measurements. After deciding on the optimized test configurations, experimental validation is undertaken on both optimized and "poor" test configurations. The results are compared with the reference parameters obtained using the conventional uniaxial testing procedures. (Appended Paper 2).

Chapter 5
In Chapter 5, a more robust optimization procedure is developed to overcome the issues revealed in the optimization study in Chapter 4. Instead of using FE simulated strain fields, the new procedure simulate the entire realistic measurement chain, including the DIC image capturing and processing. By using this method, much more uncertainties of the measurements are included into the study. (Appended Paper 3).

Based on the new optimization methodology, an effective method to reduce the random error from the measurements is proposed by studying the effect of image averaging, and an optimal number of images to be averaged is identified. Finally, a detailed experimental validation is conducted based on the optimized test configuration and other test parameters from the numerical study. (Appended Paper 4).

Chapter 6
Chapter 6 summarizes the findings of this project.

Chapter 7
Chapter 7 recommends the future work.

2. Test setup with DIC and modified Arcan fixture

2.1 Test specimen and fixture

The material chosen for the studies in this thesis to validate the developed experimental methodology is a closed-cell cross-linked Divinycell H100 PVC foam [9]. This is a polymer foam material that is widely used as core material for sandwich structures. The reason to choose the PVC foam is that detailed investigations have been carried out previously for this material to identify reliable material properties by using conventional mechanical tests. In [8] it was shown that this material has orthotropic/transversely isotropic properties due to the different lengths of the foam cells in the rising (through-thickness) and in-plane directions, respectively. This orthotropy is generated in the manufacturing process, and can be observed from microscopic images. Therefore the material principal axes are defined as the above two directions. All specimens in this study were prepared from 60 mm thick flat foam core plates.

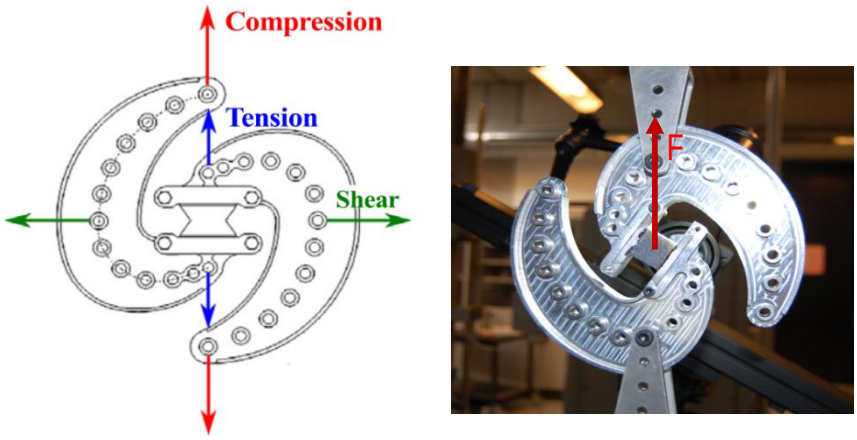

(a) *(b)*

Figure 1: *(a) Schematic of MAF rig with indication of tensile, compressive, and shear loading configurations [27]; (b) MAF rig with foam specimen subjected to combined tension/shear loading.*

In this research, a MAF fixture was used to characterize the constitutive parameters of the foam. This fixture has been developed recently to identify orthotropic material

parameters [3]. It has an S-shaped configuration consisting of two arms (shown in Figure 1). By connecting different loading holes on the arms, more complex loading conditions can be introduced compared with the conventional Arcan fixture. Besides the different combinations of shear and tensile loads, the modified Arcan fixture can also introduce pure compression or high compression to shear bidirectional loading conditions that are unable to achieve with conventional Arcan fixtures. A previous study using this modified Arcan fixture provided very reliable test results for a PVC foam material [2, 3]. However, since the PVC foam is orthotropic, the use of multiple tests to obtain the stiffness parameters is time consuming, as both through-thickness and in-plane specimens have to be prepared. Furthermore, different specimen shapes are needed to ensure a well-defined stress/strain state in the gauge area of the shear, tension and compression test specimens.

In this study there is no need to attempt to obtain homogeneous stress/strain fields, since DIC combined with the VFM allows for the identification of constitutive parameters from heterogeneous strain fields. On the contrary, heterogeneity is required for the simultaneous and accurate identification of all stiffness components. This is very important as it provides much more freedom to choose loading and boundary conditions as well as specimen geometry in the mechanical test.

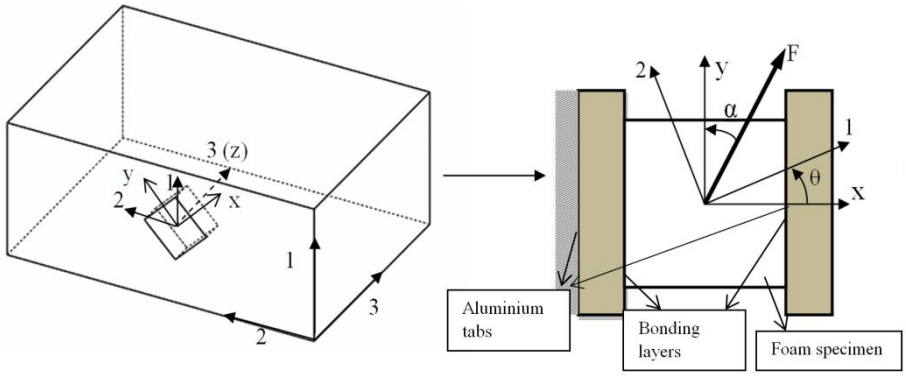

(a) *(b)*

Figure 2: *(a) Foam panel with principal material directions 1, 2 and 3; (b) Schematic of foam core specimen with Al tabs, principal material directions and load direction indicated.*

A 20 x 20 x 5 mm^3 rectangular foam block was produced to induce a heterogeneous strain field. The detailed strain maps that plotted in the following sections demonstrated that the stress state in the specimen was dominated by shear and longitudinal tensile stresses (bending). Compressive stress concentrations occur near the ends of the bonded region. Since this material has different mechanical

properties in the through-thickness (1) and in-plane (2) directions (see Figure 2 for directions), all the orthotropic stiffness components should be involved in the full deformation maps of this test. It should be noted that there is some random variations of elastic coefficients inside the foam panel due to the manufacturing process, especially towards the top and bottom surfaces of the panel [2]. Therefore, foam specimens with different off-axis angles θ were cut with high precision using a 3-axis CNC milling machine from the central part of a thick foam panel so as to avoid the inclusion of material near the top and bottom surfaces where density and stiffness variations are relatively large. Material direction 1 is the through thickness direction, and material direction 2 is the in-plane direction. After milling, the two sides of the specimens that are perpendicular to the x-axis were bonded to aluminium tabs using Araldite epoxy adhesive (indicated in Figure 2 and clearly visible in Figure 3) and fixed into the S-shape MAF rig.

2.2 DIC testing setup for the multi-axial Arcan test

2D Digital Image Correlation (DIC) was used to capture the deformation of the foam specimens. DIC is a flexible and effective technique to measure the displacements on specimen surfaces by matching the reference subsets in the undeformed image with the target subsets in the deformed image. The basic idea is that a random grey scale speckle pattern is applied onto the specimen surface using spray paint. Then by dividing each image into many small computational units called facets or subsets, the displacement can be computed at the centre of each facet by correlating the random speckle pattern. The strain components can then be obtained by numerical differentiation. A larger square facet is able to include a wider variation in grey levels and reduce the noise in the results. However, the spatial resolution is reduced when increasing the facet sizes. The detailed principle of this technique can be found in [28]. In this research, the commercial DIC system Aramis 4M [27, 29] was used to capture a series of images during deformation and to perform correlation between the deformed and undeformed images.

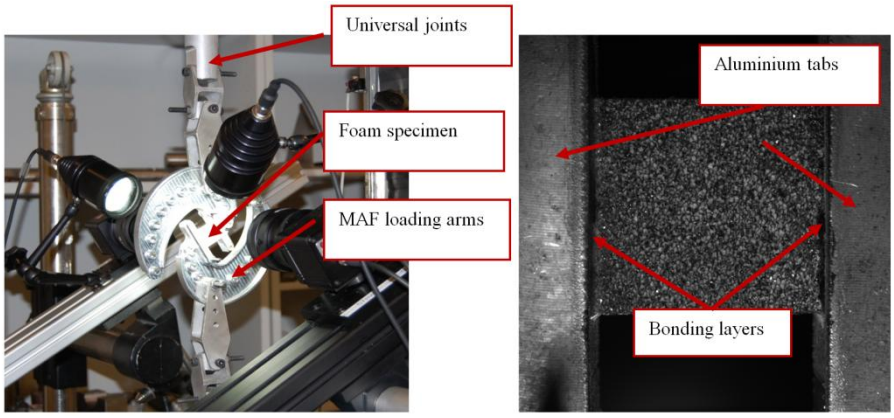

(a) *(b)*

Figure 3: *(a) DIC setup; (b) Foam core specimen with Aluminium tabs.*

A particular testing set-up (see Figure 3) was built to measure the heterogeneous deformation fields on the two back-to-back foam specimen planes. Two cameras with a resolution of 2048 x 2048 pixel^2 were placed on opposite sides of the specimen to capture the images on both sides simultaneously. The square shaped specimen was loaded multi-directionally using the Modified Arcan fixture (MAF). The cameras were rotated according to the loading angle of the specimen so that the displacements and strains were computed along the global coordinate direction of the specimen (x and y, see Figure 2). The advantage of this set-up is that it enables the elimination of out-of-plane movements by averaging the measured values from the two cameras. It can also account for possible through-thickness gradients of the strain field. This setup was already successfully employed in [30]. The detailed performance of this set-up is reported in Table 1. Resolutions were evaluated as the standard deviation of the displacement and strain maps of two consecutive images of the stationary specimen.

Table 1: *Performance report of the DIC set-up.*

Technique	2D image correlation
Subset size	Variable, to be prescribed for each set of results
Shift	50% of the subset size
Shape function	Affine
Interpolation function	Bicubic polynomial
Correlation criterion	Approximated Normalized Sum of SquaredDifference (Approximated NSSD)
Pre-smoothing applied to the images	None
Camera	8 bit, 2048 x 2048 pixel^2
Field of view	24mm x 24mm
Noise	White Gaussian, standard deviation 1% of dynamic range (2.56 grey levels)
Strain field:	
Differentiation method	Finite differences
Smoothing method	Gaussian smoothing (kernel size variable, to be précised for each set of results)

3. VFM model applied to the multi-axial MAF test

3.1 VFM – basic principles

The Virtual Fields Method (VFM) has been specifically developed for processing full-field kinematic measurements to extract parameters driving the mechanical behaviour of materials. The basic idea of the VFM is to express the condition of global equilibrium of the tested specimen using the principle of virtual work. The principle of virtual work without body forces and subjected to quasi-static loading conditions can be expressed as:

$$\int_V \sigma : \varepsilon^* dV = \int_{\partial V} \overline{T} \cdot u^* dS \tag{1}$$

where ':' denotes the contracted product of the stress tensor σ and the virtual strain tensor ε^*, and '.' denotes the dot product between the external traction force vector $\overline{T}$ and the virtual displacement vector u^*. The equation expresses the condition of global equilibrium between the internal virtual work over the specimen volume V and the external virtual work over the boundary surface of V. The only condition on the vectorial function u^* is that it is continuous and differentiable over the domain V. It is then assumed that the specimen material (polymer foam) can be described as a homogeneous, orthotropic and linear elastic solid, and that the specimen is subjected to a state of plane stress. The constitutive equations of the foam material can therefore be written as (in the material orthotropy axes):

$$\begin{Bmatrix} \sigma_1 \\ \sigma_2 \\ \sigma_6 \end{Bmatrix} = \begin{bmatrix} Q_{11} & Q_{12} & 0 \\ Q_{12} & Q_{22} & 0 \\ 0 & 0 & Q_{66} \end{bmatrix} \begin{Bmatrix} \varepsilon_1 \\ \varepsilon_2 \\ \varepsilon_6 \end{Bmatrix} \tag{2}$$

where σ_i, ε_i, (i=1,2,6) are the in-plane stress and strain components according to the so-called contracted notation [31], and Q_{ij} (i,j=1,2,6) are the in-plane stiffness components. Substituting the stress components with the actual strains and constitutive parameters, equation (1) can be rewritten as:

$$Q_{11} t \int_S \varepsilon_1 \varepsilon_1^* dS + Q_{22} t \int_S \varepsilon_2 \varepsilon_2^* dS + Q_{12} t \int_S (\varepsilon_1 \varepsilon_2^* + \varepsilon_2 \varepsilon_1^*) dS + Q_{66} t \int_S \varepsilon_6 \varepsilon_6^* dS = t \int_{Lf} (T_1 u_1^* + T_2 u_2^*) dl \tag{3}$$

where t is the thickness of the specimen. Since the elastic strain fields are known from the full-field measurement, and since the resulting force applied to the

specimen is known from the load cell readings, a new set of equations can be obtained in which only the elastic parameters are unknown for each new selected virtual field. When choosing at least as many independent virtual fields as unknowns, all the parameters can be identified directly by solving the resulting linear system [30].

For the construction of the virtual fields, piecewise functions were used in this study [32, 33]. This method uses shape functions $\Phi^{(i)}$ which are similar to those employed in finite element analysis. They express the virtual displacement $\mathbf{u}^*$ at any points in the solid as a function of the virtual displacement $u^{*(i)}$ at the nodes of a mesh as demonstrated in eq. (4):

$$\mathbf{u}^* = \sum_{i=1}^{n} \Phi^{(i)} u^{*(i)} \tag{4}$$

where n is the number of nodes per element. In the present study, bilinear shape functions with 4-noded quadrilateral elements have been used. The shape functions and nodal displacement in the element are defined as:

$$\mathbf{\Phi}: \begin{bmatrix} \Phi^{(1)} & 0 & \Phi^{(2)} & 0 & \Phi^{(3)} & 0 & \Phi^{(4)} & 0 \\ 0 & \Phi^{(1)} & 0 & \Phi^{(2)} & 0 & \Phi^{(3)} & 0 & \Phi^{(4)} \end{bmatrix} \tag{5}$$

$$\mathbf{u}^{*(i)}: \begin{bmatrix} u_1^{*(1)} \\ u_2^{*(1)} \\ u_1^{*(2)} \\ u_2^{*(2)} \\ u_1^{*(3)} \\ u_2^{*(3)} \\ u_1^{*(4)} \\ u_2^{*(4)} \end{bmatrix} \tag{6}$$

The virtual strain components in the elements are obtained by differentiating eq. (4):

$$\varepsilon^* = \sum_{i=1}^{n} S\Phi^{(i)} u^{*(i)} \tag{7}$$

where **S** is a linear differential operator defined as:

$$S:\begin{bmatrix} \dfrac{\partial}{\partial x} & 0 \\ 0 & \dfrac{\partial}{\partial y} \\ \dfrac{\partial}{\partial y} & \dfrac{\partial}{\partial x} \end{bmatrix} \tag{8}$$

As an infinite number of virtual fields can be found, an additional criterion was employed to select the virtual fields optimally and automatically aiming at minimizing noise influence on the identified parameters. The detailed derivation of this procedure is proposed in the optimized VFM theory [32]. The basic idea is to assume a Gaussian white noise added to the actual strain fields. Then the standard deviation $\sigma_{Q_{ij}}$ of each constitutive parameter Q_{ij} is directly proportional to the standard deviation $\sigma_{Q_{ij}}$ of the strain noise [33]:

$$\sigma_{Q_{ij}} = \gamma \eta_{ij} \tag{9}$$

where η_{ij} describes the sensitivity of each constitutive parameter to the noise in the VFM identification procedure. The expression of $(\eta_{ij})^2$ is derived as:

$$(\eta_{ij})^2 = \left(\frac{S}{n_p}\right)\begin{bmatrix} ((Q_{11})^2+(Q_{12})^2)\sum_{i=1}^{n_p}(\varepsilon_1^{*(ij)})^2+((Q_{22})^2+(Q_{12})^2)\sum_{i=1}^{n_p}(\varepsilon_2^{*(ij)})^2+\ldots \\ \ldots+2((Q_{11})^2+(Q_{22})^2)\sum_{i=1}^{n_p}\varepsilon_1^{*(ij)}\varepsilon_2^{*(ij)}+(Q_{66})^2)\sum_{i=1}^{n_p}(\varepsilon_6^{*(ij)})^2) \end{bmatrix} \tag{10}$$

where S is the measurement area, n_p is the amount of data points. By rewriting eq. (10), sensitivity to noise parameters can be expressed as:

$$(\eta_{ij})^2 = \frac{1}{2} Y^{*(ij)T} H Y^{*(ij)} \tag{11}$$

where $Y^{*(ij)}$ is a vector with virtual nodal displacements. H is a square matrix which contains the unknown stiffness parameters and the formulation of the virtual strain component from eq. (7). Previous work [32] has proven that $(\eta_{ij})^2$ exhibits a unique minimum. So the minimization of $(\eta_{ij})^2$ will be a criterion from which thethe virtual fields $Y^{*(ij)}$ can be chosen. The Lagrangian L associated with the constrained minimization problem can be written as:

$$L == \frac{1}{2} Y^{*(ij)T} H Y^{*(ij)} + \Lambda^{(ij)T} (A Y^{*(ij)} - Z^{(ij)}) \tag{12}$$

$\Lambda^{(ij)}(AY^{*(ij)}-Z^{(ij)})$ defines the constraints of this minimization problem. The first constraint is that the virtual field must be kinematically admissible (mainly continuity conditions). The second constraint is that the virtual field must be special so that stiffness parameters can be obtained directly as detailed definition in [32]. $I\Lambda^{(ij)}$ is a vector containing the Lagrange multipliers. A is the matrix that defines the constraints imposed. $Z^{(ij)}$ is a vector containing only zeros except one component which is equal to one. The location of this nonzero component depends on which stiffness is to be identified with this particular special field. Four optimized virtual fields are defined by solving this problem after changing the position of the 1 in the $Z^{(ij)}$ vector.

The minimization of the Lagrangian L is obtained by solving the following linear system:

$$\begin{bmatrix} H & A^T \\ A & 0 \end{bmatrix} \begin{Bmatrix} Y^{(ij)} \\ \Lambda^{(ij)} \end{Bmatrix} = \begin{Bmatrix} 0 \\ Z^{(ij)} \end{Bmatrix} \tag{13}$$

After obtaining the virtual nodal displacement vector $Y^{*(ij)}$, the unknown stiffness parameters Q_{ij} are required to determine $\square_{ij}$. The idea here is to give some initial value of Q_{ij} and to identify a first set of four special optimized virtual fields to provide updated values of Q_{ij}. Then the new Q_{ij} parameters are used in the next iteration to find the new virtual fields, etc. Previous work [32] has shown that the iterative procedure generally converges quickly within two loops regardless of the choice of initial values for the Q_{ij}.

3.2 VFM – applied to specific foam specimen and test configuration

Based on the VFM methodology described in the previous section, particular virtual fields was formulated to adapt to the current experimental set-up and specimen design. 4 x 4=16 virtual elements were employed which gives a total of 50 virtual degrees of freedom. The convergence study indicated that a 4 x 4 element size was enough to provide stable identification and save computing time compared with a higher number of virtual elements. It was found during the experiments that the aluminium tabs casted some shadow that blurred the speckle pattern and caused difficulty for DIC processing right to the edges. In addition, the adhesion used to bond the specimen and tabs might affect the accuracy of the data close to edges. Therefore, only the strain data on the area S_2 (shown in Figure 4) are used for the

VFM processing. This area has been moved slightly away from the glued specimen boundaries all the issues stated above.. The ratio between the length W of the field of view and the specimen length L is 0.95 (see Figure 4).

Therefore the area of the specimen is divided into three parts: one area with actual deformation fields being measured (S_2), and two areas without actual strain field measurements (S_1 and S_3). By separating the integrals in the principle of virtual work and assuming a state of plane-stress, equation (3) can be rewritten as:

$$-\int_{S_1} \sigma : \varepsilon^* dS - \int_{S_2} \sigma : \varepsilon^* dS - \int_{S_3} \sigma : \varepsilon^* dS + \int_{\partial S_1} \overline{T} \cdot u^* dl + \int_{\partial S_2} \overline{T} \cdot u^* dl + \int_{\partial S_3} \overline{T} \cdot u^* dl = 0 \quad (13)$$

As a consequence of the above, the virtual displacements on areas S_1 and S_3 are constrained to be rigid body-like, so that missing experimental data on these two areas will not appear in the final equation (zero virtual strain fields cancelling out the virtual work of internal forces on S_1 and S_3). Therefore, the terms related to actual stress σ on areas S_1 and S_3 should be removed in equation (14). Since no external force is applied on S_2, equation (14) becomes:

$$-\int_{S_2} \sigma : \varepsilon^* dS + \int_{\partial S_3} \overline{T} \cdot u^* dl = 0 \quad (15)$$

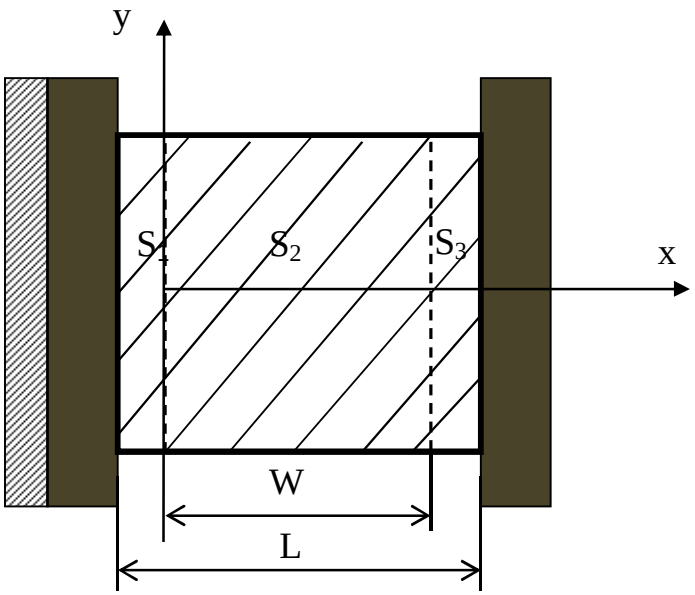

Figure 4: *Measurement area S_2 used for identification (W/L=0.95)*

The virtual displacement on S_1 is selected to be zero. For S_3, the total force F measured from the load cell can be divided into two resultant components F_x and F_y by the relation:

$$F_x = F\sin\alpha, F_y = F\cos\alpha \tag{16}$$

where α is the loading angle relative to the global coordinate direction (Figure 2). Hence the virtual work of the external forces on S_3 can be written as:

$$\int_{\partial S_3} \overline{T}\cdot u^* dl = \int_{\partial S_3} \begin{Bmatrix} f_1(y) \\ f_2(y) \end{Bmatrix} \begin{Bmatrix} u_1^* \\ u_2^* \end{Bmatrix} dl \tag{17}$$

where f_1 and f_2 are the horizontal and vertical linear force distributions along the boundaries, respectively. Since only the resultant force F is measured and the virtual displacement has to be rigid body-like on S_3, the horizontal and vertical virtual displacements on this area are defined as constants *a* and *b*. Therefore, equation (17) transforms into:

$$\int_{\partial S_3} \overline{T}\cdot u^* dl = \begin{Bmatrix} a \\ b \end{Bmatrix} \begin{Bmatrix} \int_{\partial S_3} f_1(y)dy \\ \int_{\partial S_3} f_2(y)dy \end{Bmatrix} \tag{18}$$

Since the resultant is only known in the vertical direction (direction of F in Figure 2), a good choice for *a* and *b* is:

$$\begin{cases} a = \sin\alpha \\ b = \cos\alpha \end{cases} \tag{19}$$

and the virtual work of external forces reduces to F.

In addition, the continuity conditions of the virtual displacement field lead to the following constraints on the boundary of S_2 when automatically selecting piecewise optimized virtual fields:

$$\begin{cases} u_1^{*(S_2)}(x=0,y)=0 \\ u_2^{*(S_2)}(x=0,y)=0 \end{cases} \tag{20}$$

$$\begin{cases} u_1^{*(S_2)}(x=L,y)=a \\ u_2^{*(S_2)}(x=L,y)=b \end{cases} \tag{21}$$

Since the specimens might be cut in different off-axis angles relative to the material principal directions, the actual strain and virtual strain fields should be transferred along the material principal directions from the global coordinate system when identifying the orthotropic material parameters. The transformation relation is given below.

$$\begin{Bmatrix} \varepsilon_{11} \\ \varepsilon_{22} \\ \varepsilon_{12} \end{Bmatrix} = \begin{bmatrix} c^2 & s^2 & 2cs \\ s^2 & c^2 & -2cs \\ -2cs & 2cs & 2(c^2 - s^2) \end{bmatrix} \begin{Bmatrix} \varepsilon_{xx} \\ \varepsilon_{yy} \\ \varepsilon_{xy} \end{Bmatrix} \tag{22}$$

$$c = \cos\theta, s = \sin\theta \tag{23}$$

where θ is the off-axis angle relative to the material principal direction (Figure 2).

4. Optimized experimental characterization of PVC foam based on finite element simulated strain fields

4.1 Aims and methodology

In this chapter the experimental method developed in Chapters 2 and 3 is applied to the PVC foam core material specimens to investigate the ability of the proposed methodology to identify all the elastic parameters in an actual/physical test. An extensive preliminary study has been carried out by using different test configuration, such as cantilever beam and pure shearing tests. The results indicate that the values of Q_{22} and Q_{12} change significantly when using data with different filtering levels. The most reliably determined parameters are Q_{11} and Q_{66}, which is due to the predominant longitudinal tensile and shear stresses/strains in the considered specimen. Thus it is difficult to accurately extract Q_{22} and Q_{12} from these test configurations because the transverse compressive stress/strain fields are heavily blurred by noise. The detailed results are documented in the appended Paper 1. The values of these constitutive parameters depend on different filtering techniques and the smoothing level adopted in the DIC process. Since the smoothing methodology is difficult to handle, the most feasible and efficient way to solve this problem is to modify the test configuration so that more transverse stresses/strains are introduced thus reducing the effect of noise. Therefore, a numerical optimization study is performed with different loading angles of the MAF test rig as well as different off-axis angles of the principal material axes (see Figure 2). The objective is to identify the test configuration that gives the minimum sensitivity to noise and missing data on the specimen edges, since these are the two major issues when identifying the stiffness components from actual/physical DIC measurements. After deciding on the optimized test configurations, experimental validation was undertaken on both optimized and poor (or low quality) test configurations. The results are compared with the reference parameters obtained using the conventional uniaxial testing procedures. The research reported in this chapter is documented in appended Papers 1 and 2.

4.2 Investigation of optimized test configuration

Some preliminary study with an arbitrary test configuration (pure shearing test configuration) has been done to evaluate the VFM routine developed in Chapter 3. Both the FE simulation and experimental strain fields were used to input into the VFM Matlab program. The identification results are listed in Table 2. It can be seen

that the VFM routine achieved a quite accurate identification using FE simulated strain fields. However, when the actual experimental test was performed, signification deviation was displayed, especially the identified parameters Q_{22} and Q_{12}. This problem mainly results from the reduction of the compressive zones near the loading region (as shown in Figure 5). Thus, the compressive stresses/strains are significant smaller than the predominant longitudinal tensile and shear stress/strain. Various external error sources (noise, speckle pattern, lighting, etc) cause much more difficulty in the identification procedure when using the real DIC test data which contain much more noise than the FEA generated strain fields.

Table 2: *Identified results using the FE simulated and actual experimental strain fields.*

	Q_{11} [MPa]	Q_{22} [MPa]	Q_{12} [MPa]	Q_{66} [MPa]
Identified parameters using FE simulated strain field	63.0	143	25.7	30.0
Identified parameters using experimental strain field	81.4	41.9	5.61	32.0
Reference [2]	63.4	143	26.0	30.1

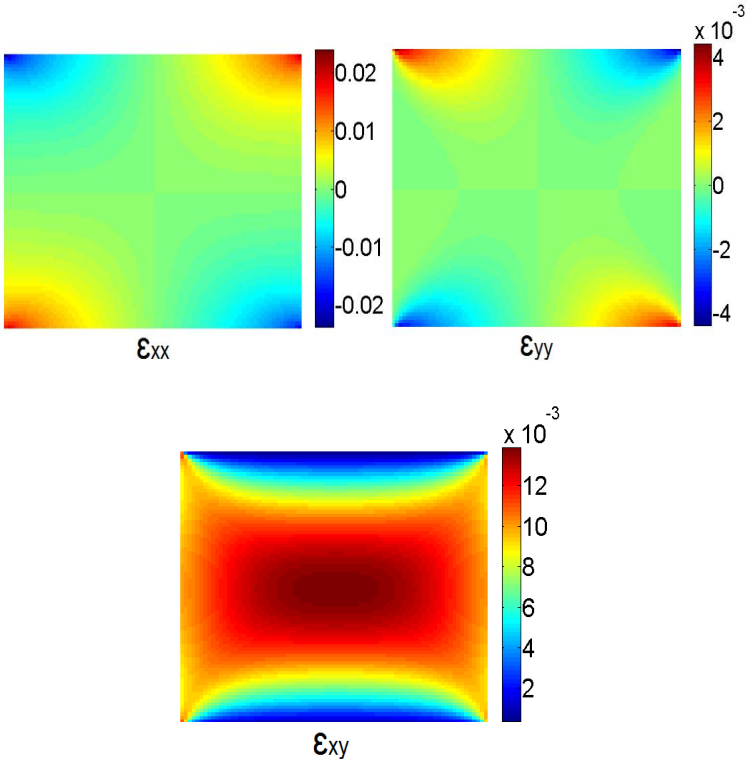

Figure 5: *The simulated strain maps using pure shearing test configuration.*

This preliminary investigation lead to the further study of the optimum test configuration so that more balanced stresses/strains are introduced thus reducing the effect of noise for all the stiffness parameters. The idea is to choose several design variables that can be easily adjusted to changes of the test configuration. Then an optimization routine is introduced to find the best combination of the design variables that leads to the best identification results. In the MAF test several design variables could be considered. The measurement area, loading angle and principal material directions are obvious variables that affect the identification performance, see Figures 2, 3 and 4. However, to ensure that the loading axis passes through the centre point of the specimen, the distance between the two bonded edges was fixed to 20 mm in this work. Therefore, the measurement area could only be varied freely along the unglued specimen sides (y direction). In order to utilize the pixels of the cameras optimally, a 20 x 20 mm^2 specimen dimension is best because it has the same aspect ratio as that of the CCD camera (2048 x 2048 pixels), as shown in [26] for a similar test configuration. As a result, the design variables selected here are the loading angle and the material principal direction (Figure 2). The loading angle can

be adjusted by connecting to different holes of the modified Arcan fixture (Figure 3). The change in material principal direction is obtained by cutting the specimen in different directions within the foam slab as demonstrated in Chapter 2 (Figure 2). FE analyses were conducted using ANSYS version 13.0 along with the ANSYS APDL language, to create 361 simulated tests with different combinations of the two design variables. The FE model is shown in Figure 6.

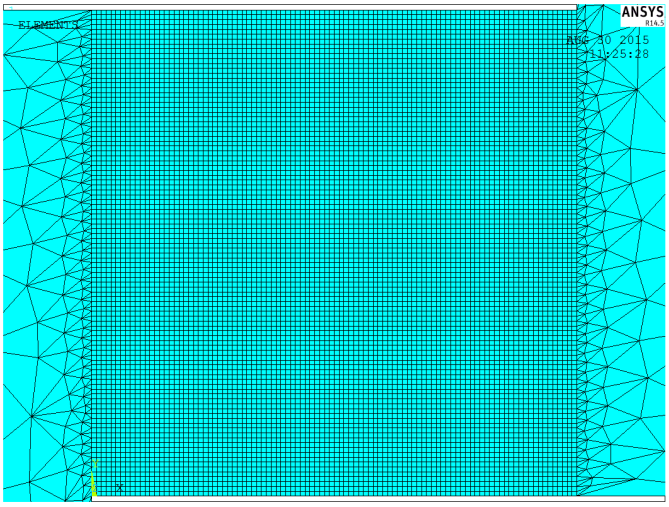

Figure 6: *FE model of foam specimen in MAF test rig.*

The FE model was built using the quadrilateral isoparametric element PLANE 82, with eight nodes and sixteen degrees of freedom (DOF). Through a thorough convergence study, a 80x80 mesh density was selected. This approximated closely the number of experimental data points (76x76), thus avoiding the introduction of any significant influence from spatial resolution differences. The number of FE simulation data points is slightly larger than the number of experimental data points, as additional data points would be removed later for studying the missing data effect. In the FE analyses, the two arms of the MAF were simulated as rigid bodies. The material principal direction was varied from 0° to 90° with increments of 5°. The load angle was varied from 0° to 90° (pure shear to pure tension) with increments of 5°. All strain maps were input into a MATLAB VFM identification routine, which was adjusted according to the loading and material angles. In the following study, two main error sources during the identification process were introduced. One is measurement noise, and the other is missing data at the edges. A cost function must be defined to describe the stability of the identified parameters with respect to the different error sources. The procedure results in plots of the cost function as a contour map with respect to the two design variables.

At the beginning, the influence of measurement noise was studied. Generally, the noise will cause the deviation of measured strain values from the exact values and certain scatter of the identified stiffness parameters. In this parametric study, the chosen cost function is identical to that used in [30] for the unnotched Iosipescu test. The sensitivity to noise parameters were used to form this cost function to find the test configuration which led to the most balanced simultaneous identification of all stiffness parameters. The relative sensitivity to the noise parameters r_{ij} used in the cost function are defined by the ratio of the sensitivity parameter η_{ij} to the corresponding stiffness parameter Q_{ij}. The detailed expression of the sensitivity parameter η_{ij} has been given in equation (14). The reason to choose the relative parameters η_{ij}/Q_{ij} instead of using the sensitivity parameter η_{ij} directly is to eliminate the influence of the order of magnitude of the different $Q_{i\ j}$ give a more clear representation of the impact of η_{ij} on the corresponding stiffness parameters. The chosen cost function C_1 is:

$$C_1 = \frac{(r_{11} - r_{22})^2 + (r_{22} - r_{66})^2 + (r_{11} - r_{66})^2}{(r_{11} + r_{22} + r_{66})^2} \tag{24}$$

In this equation, the parameter r_{12} corresponding to Q_{12} was not included in the cost function to avoid the cost function being dominated by this term which is inherently larger than the other r_{ij} parameters. The contour map of this cost function as a function of off-axis and loading angles is shown in Figure 7.

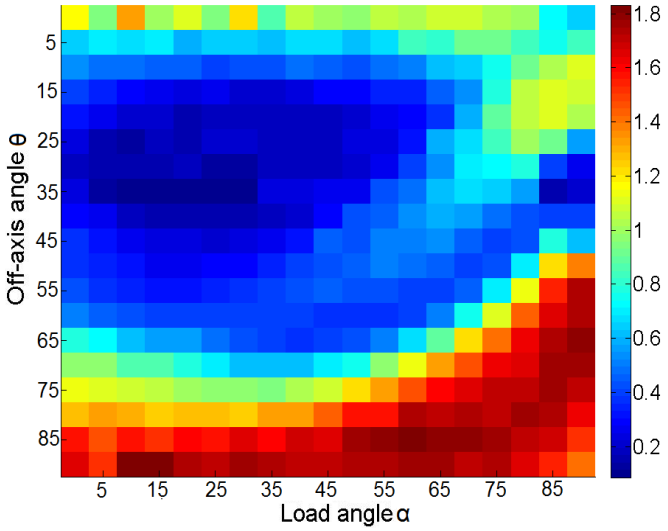

Figure 7: *Cost function for the noise sensitivity study.*

From Figure 7 it can be seen that the value of the cost function is much more dependent on the off-axis angle (also referred to as the material principal direction) than the load angle. When the material principal axes coincide with the specimen coordinate system, it is difficult to obtain an accurate identification of all four stiffness parameters regardless of the loading direction. Therefore the material principal direction is the most important factor when aiming to obtain a balanced parameter identification. The test configurations with off-axis angles between 25° and 65° provide good identification with the lowest combined sensitivity to noise. Two local minima can be observed; one is located at (θ=35°, α=30°), and the other at (θ=35°, α=85°). Since the MAF rig enables variation of the loading angle between 0° to 90° with increments of 15°, the off-axis tensile test configuration (θ=35°, α=90°) will be selected instead of the test configuration (θ=35°, α=85°).

Missing data effect

During the experimental study the missing data issue is observed around the edges of the specimen (as shown in Figure 8). It can be noted that at least half a facet size is lost at the edges of the field of view due to the intrinsic nature of the DIC algorithms. Using the smaller facet size helps reduce this influence, but unfortunately this also raises the noise level.

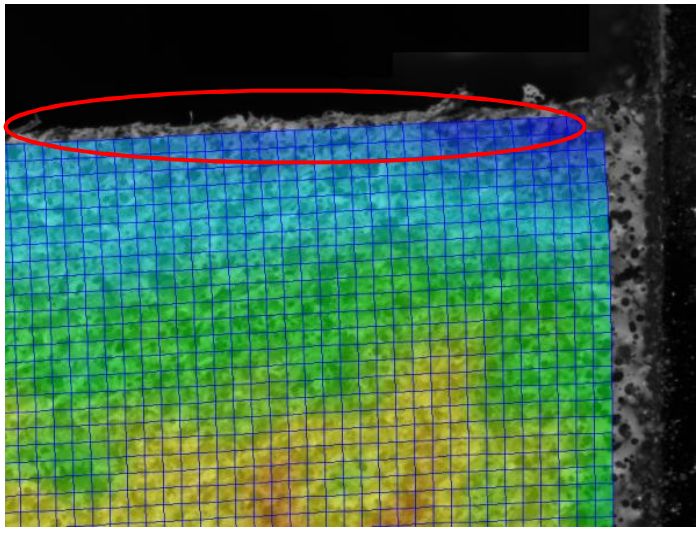

Figure 8: *The facets on the edge of the specimen.*

In the current study, two rows of data points at the top and bottom specimen edges (5% of total cross section data points) were removed in the simulated strain maps to investigate the effect of missing data. In practice, at least one row of data points at

the edges is normally incomplete and has to be deleted before inputting the strain maps into the virtual fields routine. The relative error of each of the identified stiffness parameters which is shown in Figure 9 is computed as:

$$E_{rel}(Q_{ij}) = \frac{\left|Q_{ij} - Q_{ijref}\right|}{Q_{ijref}} \tag{25}$$

where Q_{ij} is the stiffness parameter identified from the VFM routine and Q_{ijref} is the reference stiffness input into the FE model. The results shown in Figure 9 (b) indicate that missing data on the upper and bottom free edges introduces significant bias on the identified material parameters.

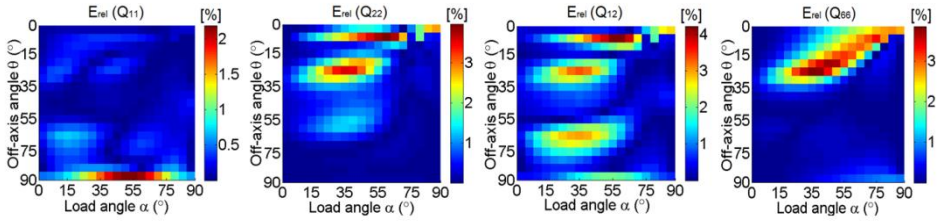

(a)

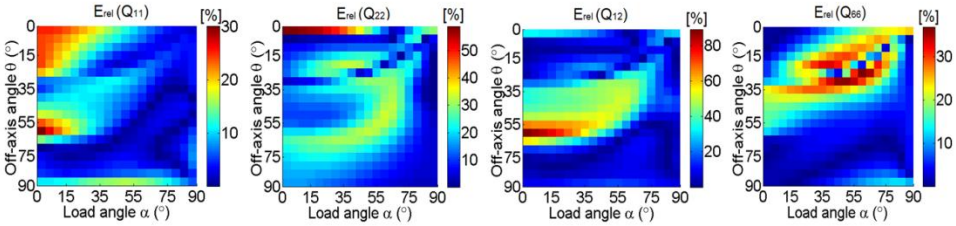

(b)

Figure 9: *(a) Relative error of each of the identified parameters with missing data on the left and right sides; (b) Relative error of each of the identified parameters with missing data on the upper and bottom edges.*

Figure (a) display the study by removing two rows of data from the right and left hand side edges. It can be seen that this missing data issue is not important on the right and left hand side edges. The main reason for this is the formulation of the VFM method given in Chapter 3. In Figure 4, the specimen was separated into 3 areas and different virtual fields were defined in these 3 areas to take into account that missing strain data on areas S_1 and S_3. Since the virtual displacements on S_1 and S_3 are set to be rigid body motions, the principle of virtual work is expressed as

given in eq. (15). However due to the missing data on the up and bottom free edges, the actual strains are also not available in the areas S_4 and S_5 shown in Figure 10. Thus, eq. (15) can be rewritten as:

$$-\int_{S_2} \sigma : \varepsilon^* dS - \int_{S_4} \sigma : \varepsilon^* dS - \int_{S_5} \sigma : \varepsilon^* dS + \int_{\partial S_3} \overline{T} \cdot u^* dl = 0 \qquad (26)$$

where $\int_{S_4} \sigma : \varepsilon^* dS$ and $\int_{S_5} \sigma : \varepsilon^* dS$ are the error terms introduced by the missing data effect. It would be possible to assign rigid body-like virtual fields to S_4 and S_5 as well, but the continuity conditions on the virtual displacements would then make it impossible to include the applied force in the equation. Thus, it would only be possible to identify stiffness ratios, not actual stiffness values. Therefore the VFM identification area can be easily adjusted in the horizontal direction when missing data at the left and right edges. However, if data are missing at the top and bottom edges, this means that the fraction of the shear/tension force going through this section will be missing in the equilibrium equation, resulting in significant overestimation of the stiffnesses as seen from Figure 9 (b).

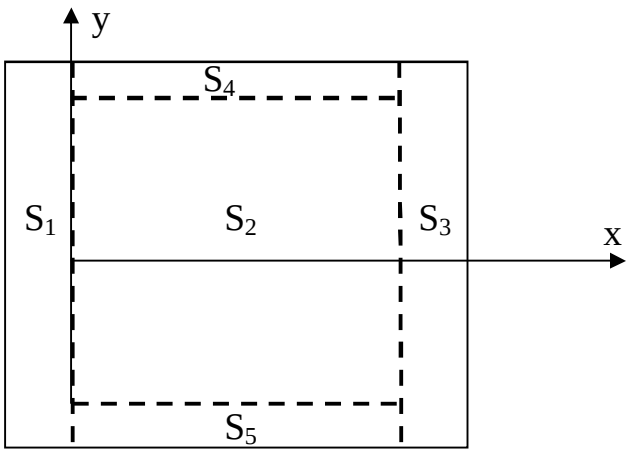

Figure 10: *The measurement area S_2 used for identification with missing data on free edges.*

A new cost function C_2 was defined to represent the overall identification error with missing data on the free edges, and is given as:

$$C_2 = \sqrt{\left(\frac{Q_{11}-Q_{11ref}}{Q_{11ref}}\right)^2 + \left(\frac{Q_{22}-Q_{22ref}}{Q_{22ref}}\right)^2 + \left(\frac{Q_{12}-Q_{12ref}}{Q_{12ref}}\right)^2 + \left(\frac{Q_{66}-Q_{66ref}}{Q_{66ref}}\right)^2} \quad (27)$$

In eq. (27) Q_{ijref} are the reference values of the four identified material stiffness parameters, and Q_{ij} are the identified parameters affected by missing data. The plot of this cost function contour map according to different test configurations is shown in Figure 11. It corresponds to 5% missing data. The results show that the missing data effect significantly affects the identification results on lots of different test configurations. For some shear and biaxial loading test configurations, the overall identification error of the four stiffness parameters becomes extremely significant. This is due to that a bending moment is gradually induced when the loading angle is increased. The bending moment produces large bending stresses at the free edges, resulting in a more significant error on the equilibrium equation when data points are missing there. Therefore, the minimal identification error is obtained around the tensile test configuration.

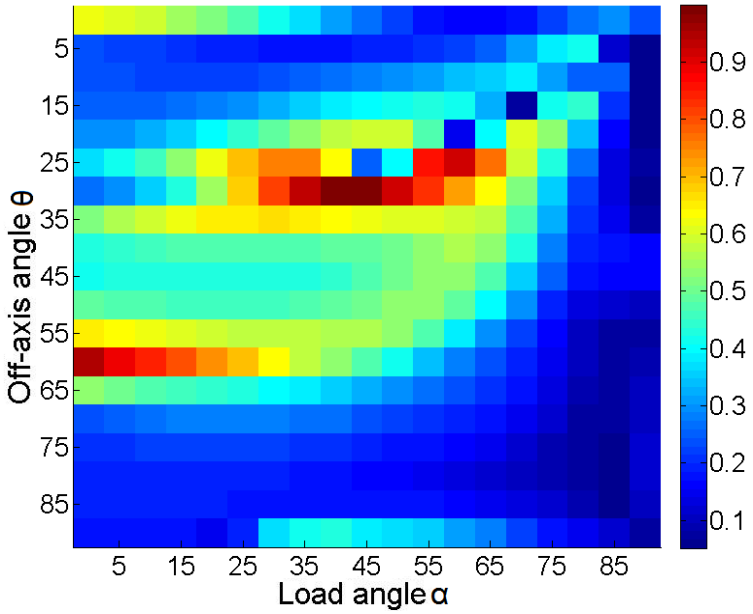

Figure 11: *The cost fuction for missing data sensitivity study (5% of total data missing).*

In order to further validate the optimized test configuration, the cost function contour was created by increasing the amount of missing data to 20% (shown in Figure 12). The overall identification error for the four stiffness parameters increases significantly compared with the results in Figure 11. Although there is a slight variation between the patterns of the two cost function plot, the best areas (around tensile loading angle) of these two contours are still very stable and consistent. It should be noted that what appear to be singularities occur at several locations in Figure 11 (θ=25° and α=45°, etc). But at the same time the number of 'singular points' is greatly reduced in Figure 12, even though they tend to occur in the same location of the design space. The main reason for this is that some 'poor' test configurations are very sensitive to the missing data effect. So the results produced by these 'poor' test configurations are very unstable and easily affected by the amount of missing data. The experimental study in the next section also indicates that these 'poor' test configurations are very sensitive to the virtual field mesh sizes. Therefore, a more reliable way to select an optimized test configuration is to look for the locations/spots and their near vicinity with the lowest value of the cost function.

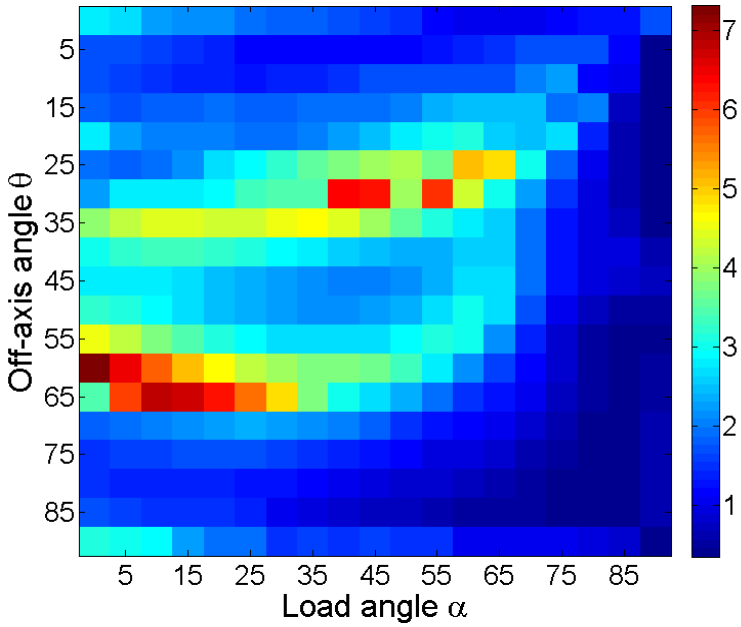

Figure 12: *The cost fuction for missing data sensitivity study (20% of total data missing).*

In order to reduce the missing data effect on the identification procedure demonstrated above, the missing data points at the two free edges were reconstructed by extrapolating the 2D data (strain) maps. The idea is to use the nearest data points and to copy them to the missing data positions ('padding' procedure). The cost function contour map after conducting this extrapolation is shown in Figure 13. The maximum value is around 0.12, which is much smaller than the value shown in Figure 11. This indicates that much improved parameter identification can be achieved when the missing data have been recovered. The plot in Figure 13 also indicates that the "poor" test configurations represented by the central part of the cost function map shown in Figure 11 experienced significant improvement when missing data recovery was performed. Nevertheless, choosing a test configuration which can give less sensitivity to missing data is still important even with the extrapolation of 2D data maps. Combining this result with the conclusion derived from the noise sensitivity study, it is found that the best test configuration to minimize the noise effect displayed in Figure 7 is around θ=35° and α=30°, while the best configuration to minimize the missing data effect is around θ=35° and α=90°. Therefore a compromise between these two factors has to be made in the actual/physical test. By combining the plots in Figures 7, 11 and 13 it is found that θ=35° and α=90° provides the best compromise. Therefore this configuration has been selected for the experimental validation. Another good test configuration is the biaxial loading test with θ=35° and α=30°. The reason that this test configuration was also selected for the experimental validation is that it has the minimal cost function value when only noise is considered (see Figure 7). Thus, if the error from missing data can be reduced to a very low level, this test configuration should provide the best parameter identification. A comparison of these two configurations will provide insight into the real practical effect of missing data.

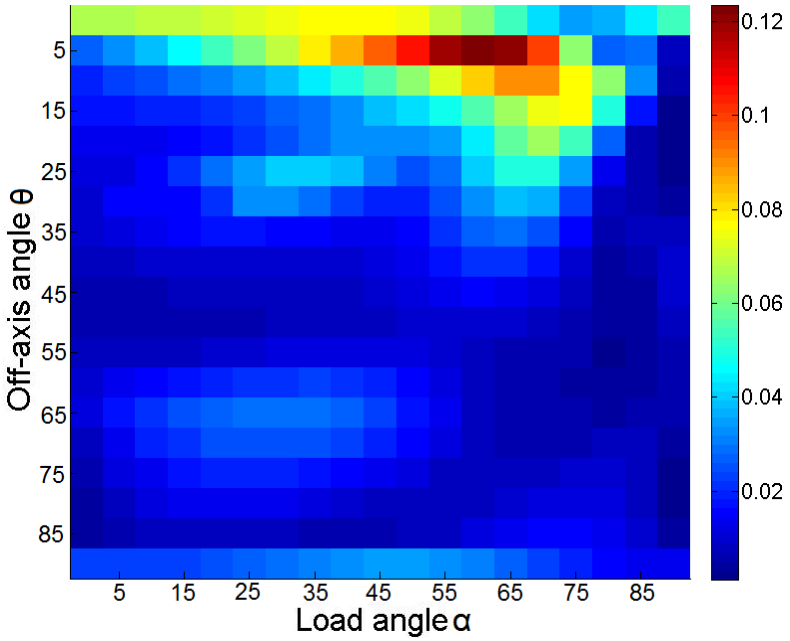

Figure 13: *Cost function with extrapolation of missing data*

4.3 Experimental validation and discussion

In order to validate the above findings from the numerical optimization study, several experimental study has been conducted. The two optimized test configurations selected from chapter 4.1 have been used to compare with the pure shear test configuration investigated in the preliminary study (θ=90°, α=0°). Reference values for the elastic properties were obtained using ASTM standard tests in [8], as well as from measurements conducted using the MAF jig with tensile tests along the in-plane and through-thickness directions and shearing tests using butterfly-shaped specimens [2]. Figure 14 shows the strain maps for the pure shear test given in the material orthotropy axes. The load is applied to the foam specimens up to around 150 N in 5 load steps. The strain maps are derived within the linear elastic region based on the previous study [1] of the tensile and shear stress vs. strain curves until failure using classical mechanical testing method. The constitutive parameters identified for the 4 foam specimens are listed in Table 3. The relative difference is given by comparing the average testing results and the mean value of two sets of reference data [2, 8]. It is observed from the results that the most reliably determined constitutive parameters in the pure shear loading test configuration are

Q_{22} and Q_{66}, which is due to the predominant longitudinal bending and shear stresses/strains in the specimen. At the same time, it is difficult to extract Q_{11} and Q_{12} from this (pure shear) test configuration because of the very low levels of transverse stress. Thus, Q_{11} and Q_{12} exhibit a large bias even when applying the extrapolation on the edges of the data maps.

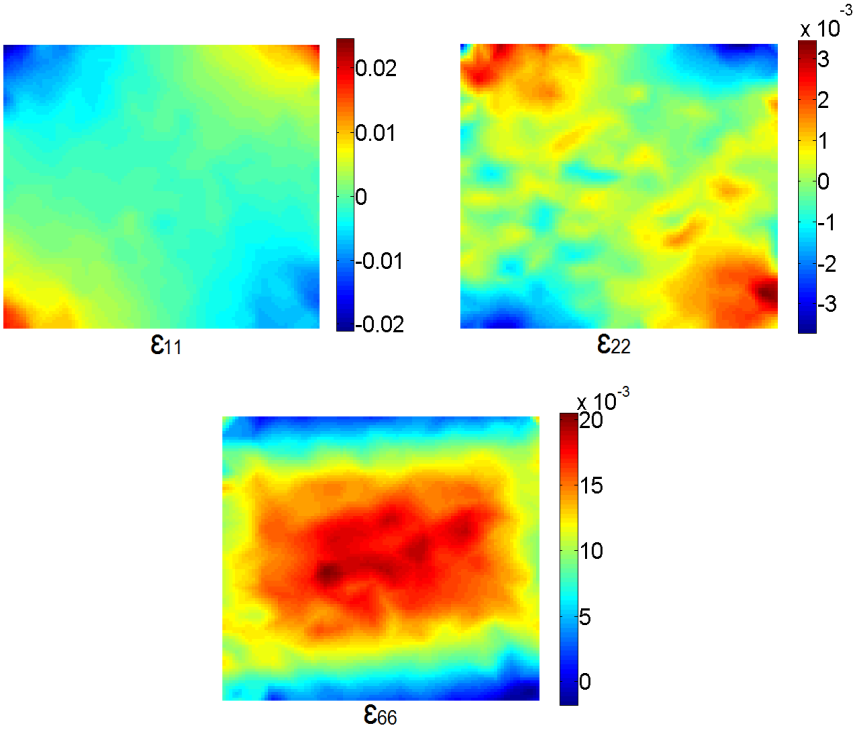

Figure 14: *DIC strain maps for the θ=90° and α=0° test configuration (pure shear).*

Table 3: *θ=90° and α=0° - pure shear test configuration.*

	After Extrapolation				**Before Extrapolation**			
[MPa]	Q_{11}	Q_{22}	Q_{12}	Q_{66}	Q_{11}	Q_{22}	Q_{12}	Q_{66}
Test1	20.3	73.4	4.15	28.7	59.5	83.5	19.0	29.0
Test2	1.06	66.0	0.01	30.6	12.9	78.0	2.33	32.5
Test3	13.0	71.3	2.35	32.1	43.0	80.9	11.1	34.9
Test4	3.44	70.0	0.670	32.0	20.7	80.2	6.06	33.4
Average	9.45	70.2	1.80	30.9	34.0	80.6	9.63	32.5
Ref(AAU) [2]	140	63.5	23.6	32.5	140	63.5	23.6	32.5
Ref(SOU) [8]	143	63.4	26.0	30.1	143	63.4	26.0	30.1
Relative Difference	93.3%	10.6%	92.4%	1.28%	75.7%	26.9%	59.2%	3.83%

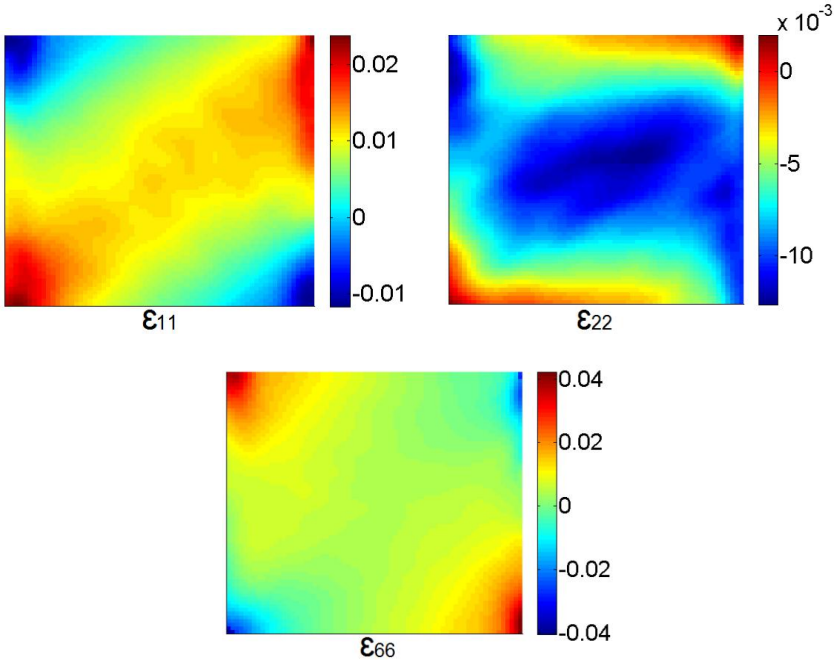

Figure 15: *DIC strain maps for the θ=35° and α=30° test configuration (multi axial loading).*

Table 4: *θ=35° and α=30° - multi-axial test configuration.*

After Extrapolation					**Before Extrapolation**			
[MPa]	Q_{11}	Q_{22}	Q_{12}	Q_{66}	Q_{11}	Q_{22}	Q_{12}	Q_{66}
Test1	156	73.9	11.1	35.5	165	101	19.8	46.3
Test2	152	77.3	9.98	34.6	159	94.2	14.7	43.6
Test3	158	81.0	11.3	34.0	170	101	19.3	45.9
Test4	148	69.2	8.05	33.6	158	88.6	13.2	40.6
Average	154	75.4	10.1	34.4	163	96.2	16.7	44.1
Ref(AAU)[2]	140	63.5	23.6	32.5	140	63.5	23.6	32.5
Ref(SOU)[8]	143	63.4	26.0	30.1	143	63.4	26.0	30.1
Relative Difference	8.83 %	18.8 %	59.2 %	9.90 %	15.2 %	51.5 %	32.7 %	40.9 %

Figure 15 and 16 demonstrated the strain maps obtained using the biaxial test configuration (θ=35° and α=30°) and the off-axis tensile test configuration (θ=35° and α=90°). The identification results are listed in Table 4 and 5. As observed from the DIC strain maps obtained, the two optimized positions gave much more balanced strain values for all components with non-zero values over most of the field of view (Figure 15 and 16), whereas in the pure shear test, most of the significant normal strain values are concentrated at the corners (Figure 14). Hence, the accuracy of the identified parameters with two optimized test configuration is significantly improved compared with the results using pure shear test. For the results without any data extrapolation on the edges to recover missing data, the off-axis tensile test gives much more accurate results than the biaxial test, especially for the stiffness parameter Q_{22}.

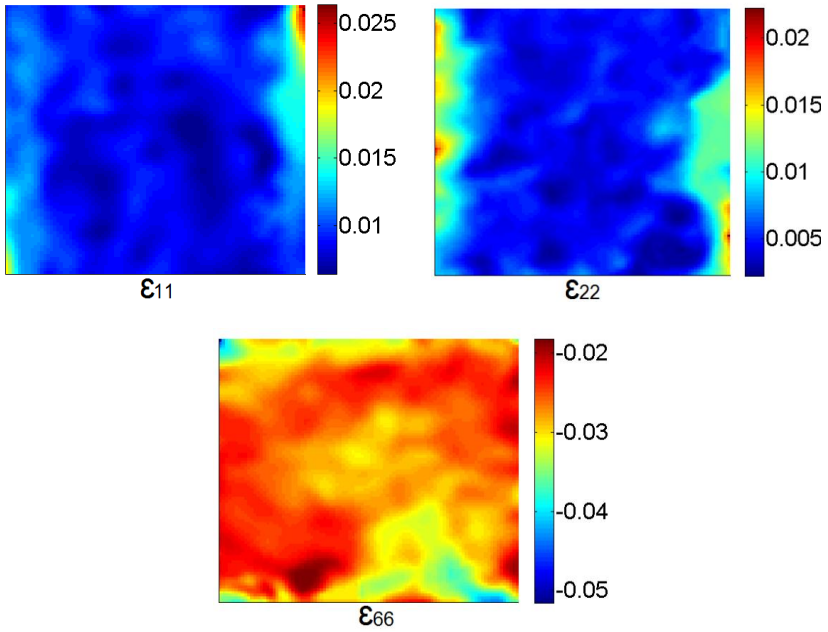

Figure 16: *DIC strain maps for the θ=35° and α=90° test configuration (off-axis tensile).*

By correcting the missing data on the upper and bottom edges of the specimen, the results from both test configurations was brought much closer to the reference values. This is consistent with the findings of the simulation study demonstrated in Figure 11. However, the variation before and after correcting the missing data is much smaller for off-axis tensile test compared with the results of the biaxial test. To further evaluate the two optimized test configurations, different virtual field element mesh sizes were used to extract the stiffness parameters from the DIC strain data. Table 6 and Table 7 show the comparison between the two test configurations using different virtual field mesh sizes. It is observed that the results of the off-axis tensile tests are much more stable than those obtained from the off-axis multi-axial test, especially for the identification of the parameters Q_{22}, Q_{12} and Q_{66}. The most stable parameter identified in the current test is Q_{66}. This was expected since off-axis tensile tests induce very large shear strains, and such test configuration is therefore commonly used to determine the in-plane shear modulus of anisotropic materials [34]. The major limitation of the standard off-axis tensile test is that it is very hard to produce a homogeneous stress/strain distribution in the specimen gauge section. However by using DIC and VFM this problem is solved. By comparing the strain maps from these two test configurations (Figure 15 and 16), it can be noted that the off-axis tensile test provides much less spatial heterogeneity. That is the major

reason why this test configuration leads to the best and most stable results. As a consequence, the limited spatial resolution of DIC has less impact on the strain maps for this test than for the biaxial configuration.

Table 5: *θ=35° and α=90° - off-axis tensile test configuration.*

After Extrapolation					**Before Extrapolation**			
[MPa]	Q_{11}	Q_{22}	Q_{12}	Q_{66}	Q_{11}	Q_{22}	Q_{12}	Q_{66}
Test1	144	75.4	19.4	29.5	147	77.3	20.9	30.6
Test2	152	78.8	19.0	31.6	157	84.2	19.7	33.6
Test3	148	78.0	20.1	31.3	150	81.1	21.3	31.9
Test4	150	71.2	18.0	28.2	153	74.6	18.2	30.6
Average	148	75.9	19.1	30.2	152	79.3	20.0	31.7
Ref(AAU)[2]	140	63.5	23.6	32.5	140	63.5	23.6	32.5
Ref(SOU)[8]	143	63.4	26.0	30.1	143	63.4	26.0	30.1
Relative Difference	4.59 %	19.5 %	23.0 %	3.51 %	7.42 %	25.0 %	19.4 %	1.28 %

Table 6: *θ=35° and α=30° - muti-axial test configuration with different virtual field mesh sizes.*

[MPa]	***Mesh 4x4***	***Mesh 6x6***	***Mesh 10x10***	***Ref(AAU)***	***Ref(SOU)***
Q_{11}	156	155	150	141	143
Q_{22}	73.9	50.8	35.7	63.5	63.4
Q_{12}	11.1	6.61	3.02	23.6	26.0
Q_{66}	35.5	29.7	21.4	32.5	30.1

Table 7: *θ=35° and α=90° - off-axis tensile test configuration with different virtual field mesh sizes.*

[MPa]	***Mesh 4x4***	***Mesh 6x6***	***Mesh 10x10***	***Ref(AAU)***	***Ref(SOU)***
Q_{11}	144	138	136	141	143
Q_{22}	75.4	66.5	58.7	63.5	63.4
Q_{12}	19.4	27.8	31.6	23.6	26.0
Q_{66}	29.5	29.9	30.2	32.5	30.1

Although the off-axis tensile test gives a relatively reliable identification, there are still some differences between the identified parameters and the reference values. Significant density variations exist within the tested PVC foam panels, and this may account for some of the differences observed. However, the significant variations observed for Q_{22} and Q_{12} when the virtual field mesh size is varied indicate that there are some unresolved issues in the present methodology. This thought leads to a further investigation in order to set up a more realistic simulation of the identification procedure to track all possible sources of bias, and based on this to choose regularizing parameters (subset size, smoothing) in a more rational way. This part of study will be report in the next Chapter.

5. Optimization study by simulating the entire measurement chain

5.1 Aims and methodology

Although the selected test configuration in Chapter 4 demonstrates the capability of extracting the full set of elastic stiffness parameters, several issues still bring uncertainty to the identified results. The investigation in Chapter 4 highlighted that one of the reasons for this was that the optimization study was based on finite element simulated strain fields, which did not include the sources of error that arise from real DIC measurements. In particular, the low-pass spatial filtering effect of the DIC measurements will result in underestimation of the strains in large strain gradient areas of the test specimen, which in turn will lead to biases on the identified stiffness components. Moreover, the low signal to noise ratio associated with the measurement of the elastic material properties of polymer foams will tend to increase the random error (scatter) of the data. These unresolved issues led to the work described in this chapter, aiming to establish a method for quantifying the uncertainty of the measurements and to further improve the experiments.

A procedure has been developed to realistically simulate the MAF test for polymer foams using DIC and the VFM. The idea is to construct deformed synthetic images using displacements generated from FE analyses. From this, the reference and deformed synthetic images will be processed using DIC, and VFM will be used subsequently to extract all the stiffness parameters. The uncertainty of the measurements, including the systematic and random errors, has been evaluated thoroughly by including several different sources of error. The systematic and random errors of the measurements were analyzed separately by introducing two different error functions based on data with and without simulated camera noise. The optimization study was undertaken by using the loading angle and the off-axis angle relative to the material principal direction as the two design variables. By minimizing the uncertainty predicted from the error functions, an optimized test configuration has been identified. Subsequently, the influence of subset size and smoothing levels has been evaluated based on the optimized test configuration. Moreover, an effective method to reduce the random error from the measurements has been proposed by studying the effect of image averaging, and an optimal number of images to be averaged has been identified. Finally, a detailed experimental validation has been conducted based on the optimized test parameters selected from the numerical study. The research reported in this chapter is documented in appended Papers 3 and 4.

A simulator tool has been developed to produce optimal test configurations to identify mechanical constitutive parameters from full-field measurements and inverse identification using the VFM. Figure 17 illustrates a flowchart of the developed simulator. It is seen from the measurement chain depicted in Figure 16 that the identification accuracy depends on many parameters. Some of these are selected by the operator in an intuitive way, like e.g. the types of cameras or subset sizes. Others parameters are often overlooked such like the parameters hidden in commercial DIC packages (the shape functions or the interpolation functions), or the speckle pattern which is often produced in a non-optimized nor reproducible manner with paint spray. For future wider and possibly industrial application of this new test methodology, it is essential to be able to quantify the uncertainty of all the parameters in the grey boxes mentioned in Figure 17 (and there are others not mentioned like the effect of lighting or the lens quality for instance) to produce the most robust results. Since addressing this complex optimization problem with all parameters included is out-of-reach, the research conducted in this study focuses on a few parameters considered to be the most influential: the subset size, the strain smoothing kernel as well as the two test design variables (loading and off-axis angles).

As stated in the GUM (Guide to the expression of Uncertainty in Measurement, [35]), the uncertainty of a measurement result is usually evaluated using a mathematical model of the measurement and the law of propagation of uncertainty. This is the principle undertaken in this study. Two main sources of uncertainty are defined in the GUM: type A, which relates to the random part of the uncertainty and can be evaluated with statistical parameters, and type B which relates to systematic errors or biases. In the rest of the thesis, type A uncertainty will be named ‘random error’, whereas type B will be called ‘systematic error’ or ‘bias’.

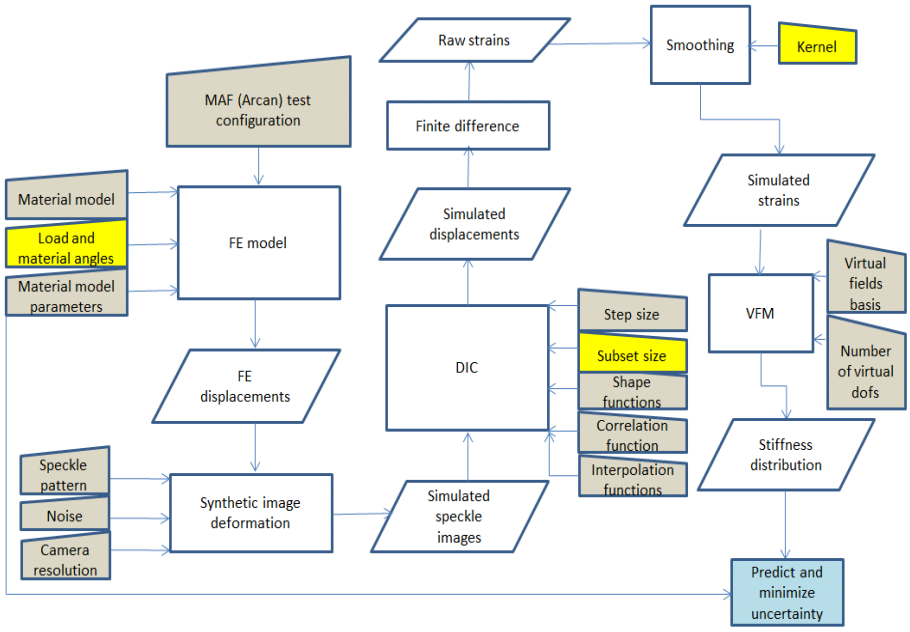

Figure 17: *Flowchart of the developed identification simulator (in grey, fixed parameters, in yellow, parameters studied here)*

Two error functions were defined to evaluate the systematic and random errors separately. The hypothesis is that minimization of the systematic and random errors will make it possible to specify a set of design variables that will provide the best identification of the materials parameters. In order to simplify the problem, the optimization will be conducted in two steps. First, the two test design variables (the loading angle and the off-axis angle relative to the material principal direction) will be chosen to achieve the overall minimal systematic and random errors. After deciding on these, the optimization of the image processing parameters will be conducted to further improve the material parameter identification. The procedure is similar to the optimization study conducted on the test configurations except that the DIC subset and smoothing kernel sizes are considered as the new design variables, while the test configuration has been selected based on the first step. Finally, an efficient method to reduce the random error is proposed in which multiple stabilized images are captured and then averaged. An optimal number of images will be defined based on this study.

As stated in Chpater 3.2, the DIC measurement data near the edges of the specimen may be influenced by the adhesive or the shadow cast by the MAF fixture (see Figures 2 and 3). The way to solve this issue is similar to the procedure presented in Chapter 3.2, and henceforth will not be described in detail here. Only the

measurement area S_2 is taken into account in this VFM study (shown in Figure 18). The ratio between the length *W* of the field of view and the specimen length *L* is 0.8. It It is important not to reduce this value too much as this would result in a loss of strain heterogeneity which would negatively impact the simultaneous identification of the complete set of stiffness components.

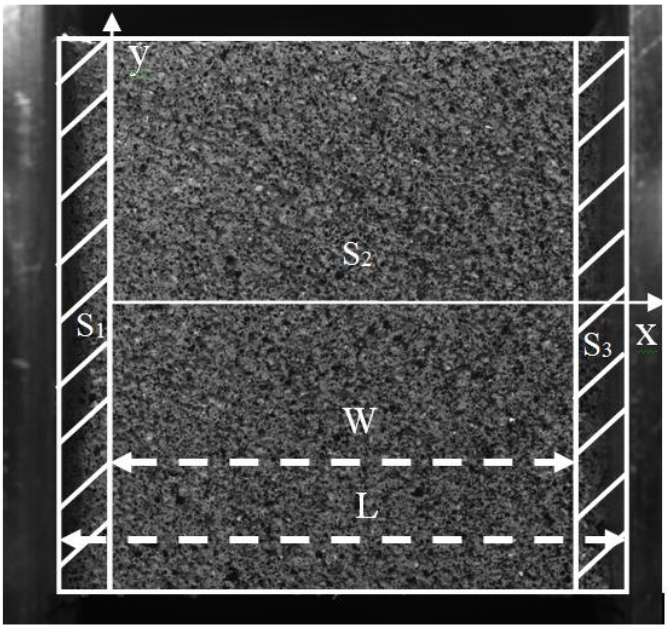

Figure 18: *Measurement area S_2 used for identification (W/L=0.8).*

More details of the derivation of the virtual boundary conditions can be found in Chapter 3. For the identification of the orthotropic material parameters, the strain and virtual strain fields obtained in the global coordinates x and y (see Figure 2) were transformed into the material principal directions 1 and 2 (Figure 2). The transformation relations are given in Equations (22) and (23) given in Chapter 3.

5.2 DIC simulator

An important improvement of this new optimization study compared with the previous work in Chapter 4 is to simulate the DIC process realistically. The procedure includes three steps: (1) Development of a FE model to create the displacements field; (2) Superimpose the reference images with displacements obtained from the FE analysis; (3) DIC between the reference and deformed synthetic images. The parametric FE analysis was performed using ANSYS version 14.0 together with the ANSYS APDL language to simulate the MAF specimen response with different test configurations. The reference material properties (Q_{11}=143.4 MPa, Q_{22}=63.41 MPa, Q_{12}=26.01 MPa, Q_{66}=30.12 MPa). The details of the FE model were described in Chapter 4.

The FE simulated displacement fields were generated with different combinations of the two design variables (the loading angle and the material principal direction). After obtaining the FE displacement fields, a synthetic deformation procedure of the speckle patterns was adopted to simulate the image recording process. The reference image, captured from one of the test specimens in real testing conditions, is shown in Figure 19(a). The reference image was deformed according to the displacement fields calculated from the FE model. The deformation process was performed numerically using an interpolation routine. This procedure is based on the 2D interpolation functions in Matlab, and it was proposed and validated previously [36]. Figure 19(b) shows an example of the deformed synthetic images for a specimen configuration subjected to pure shear loading. The synthetic images were processed by the MatchID DIC software [37, 38] to calculate the displacement fields, and the strain fields were subsequently derived using finite differences and subsequent Gaussian smoothing. The advantage of this DIC software compared with other commercial software is that users can write their all own scripts to control all the parameters inside DIC process (subset size, shift, measurement areas, etc). This feature can be embedded with Matlab code to perform parametric study and find the optimum DIC parameters. The details of this study will be reported in the following sections. Table 8 summarizes the parameters used for DIC.

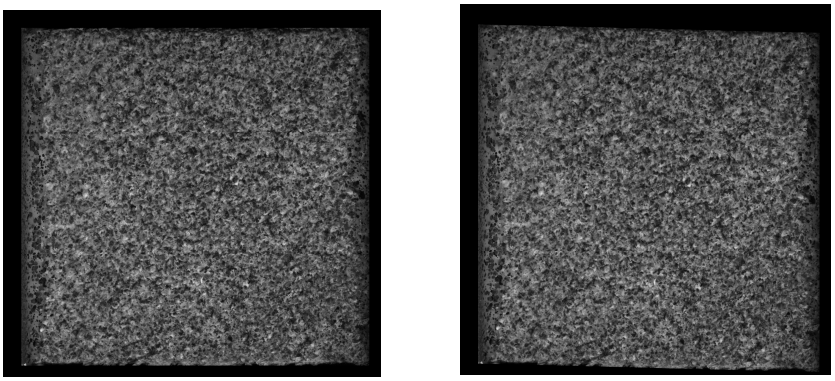

(a) *(b)*

Figure 19: *(a) Reference image (size 1650 x 1650 pixel^2); (b) Deformed synthetic image for a vertical shear load.*

Table 8: *DIC parameters for the numerical study (MatchID DIC package).*

Technique	2D image correlation
Subset size	Variable, to be precised for each set of results
Shift	50% of the subset size
Shape function	Affine
Interpolation function	Bicubic polynomial
Correlation criterion	Approximated Normalized Sum of Squared Difference (Approximated NSSD)
Pre-smoothing applied to the images	None
Camera	8 bit, 2048 x 2048 pixel^2
Field of view	24mm x 24mm
Noise	White Gaussian, standard deviation 1% of dynamic range (2.56 grey levels)
Strain field:	
Differentiation method	Finite differences
Smoothing method	Gaussian smoothing (kernel size variable, to be précised for each set of results)

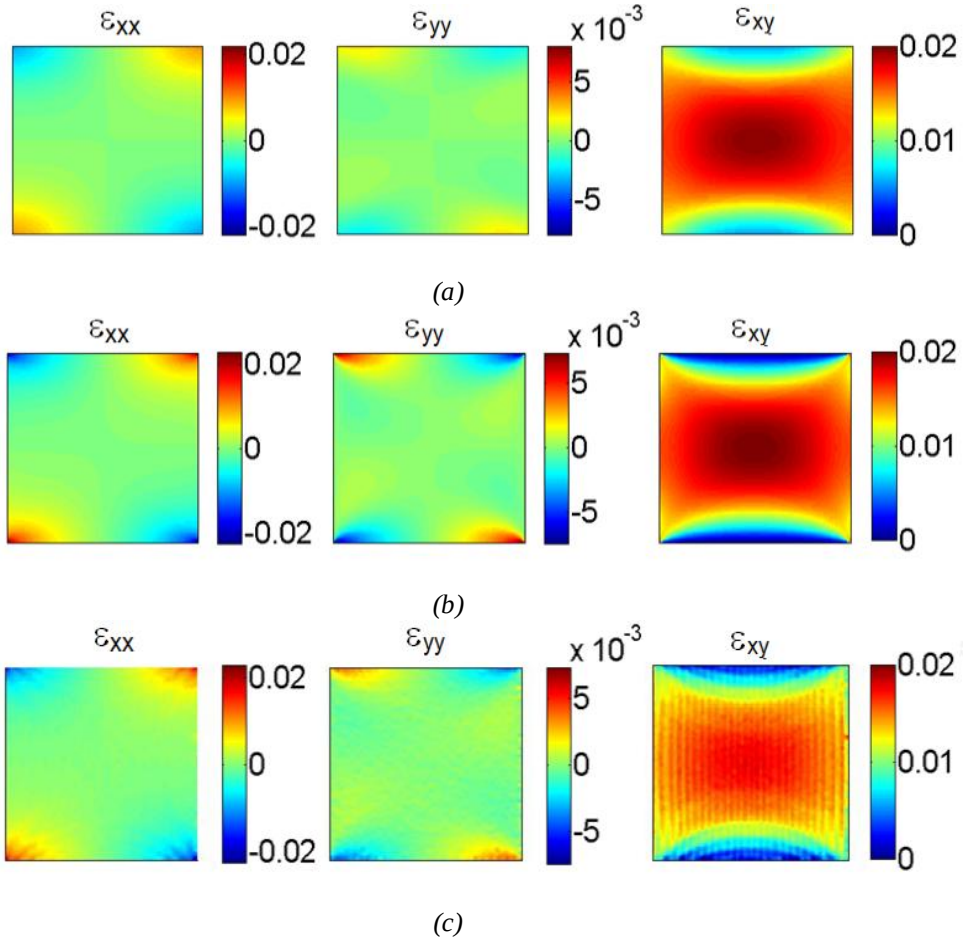

Figure 20: (a) Strain maps from DIC using synthetic images without noise (Subset size: 30, Gaussian kernel size: 10); (b) Strain maps from FE model; (c) Strain maps from DIC using synthetic images without noise (Subset size: 30, Gaussian kernel size: 2).

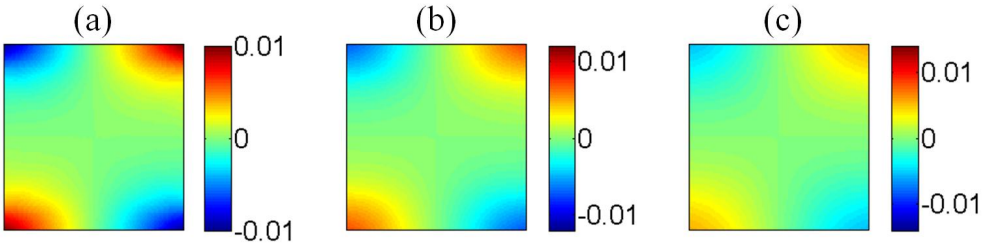

Figure 21: ε_{xx} strain maps with Gaussian kernel size of (a) 10; (b) 20; (c) 30.

This systematic reconstruction bias is an important source of error which has to be taken into account in order to predict the identification error realistically. For test configurations which result in more severe strain gradients, the low-pass filtering effect of DIC will be more critical and lead to significant errors in the parameter identification. A detailed study of this is presented in the following section.

5.3 Test optimization based on the systematic error

With the simulated experimental procedure described previously, it is possible to quantify the systematic error caused by DIC process for different test configurations. By using the similar parametric study approach stated in Chapter 4, the FE displacements were obtained by using different combinations of the two design variables of the test configuration (the material principal direction and the loading angle). The material principal direction (θ – see Figure 2) was varied between 0° to 90° with increments of 5°. The loading angle (α – see Figure 2) was also varied between 0° to 90° (from pure shear to pure tension) with increments of 15° according to the MAF test jig, see Figures 1 and 2. However, instead of inputting the FE deformation fields into the VFM routine to study the optimized test configuration, the FE simulated displacements were imposed on the reference speckle pattern by using the DIC simulator introduced in the previous section, synthetic deformed images corresponding to different test configurations were produced. Since only the systematic error is considered in this section, noise was not added to the synthetic images. The reference and deformed synthetic images were processed by the DIC software run in batch mode to calculate the new simulated DIC displacement fields. A subset size of 30 x 30 was selected here. After this the strain maps were derived by numerical differentiation with Gaussian smoothing with a kernel size of 10. Based on the tensile and shear stress vs. strain curves until failure obtained from previous work [1], the strain maps are restricted to the linear elastic region of the PVC foam. Based on the experience from the study in Chapter 4, the random error is highly dependent on the signal to noise ratio. Therefore, it is beneficial to achievestrains that are as large as possible. However, this is limited in practice by the fact that the material needs to remain linear elastic. Moreover, different test configurations (off-axis and load angles) lead to different stiffnesses, so in order to provide an unbiased comparison, it is necessary to normalize the applied load by a scaling factor *k* defined here as:

$$k = \max\left[\max\left|\frac{\varepsilon_x^i}{\varepsilon_x^{\max}}\right|, \max\left|\frac{\varepsilon_y^i}{\varepsilon_y^{\max}}\right|, \max\left|\frac{\varepsilon_{xy}^i}{\varepsilon_{xy}^{\max}}\right|\right] \tag{28}$$

where $\varepsilon_x^i, \varepsilon_y^i$ and ε_{xy}^i are the strain components at i'th data point of the model. Max |.| is the maximum absolute value over all the data points, and $\varepsilon_x^{\max}$, $\varepsilon_y^{\max}$ and $\varepsilon_{xy}^{\max}$ are the maximum allowable strain values for the material to remain linear elastic. These were obtained from previous experiments with standard mechanical test methods and reach up to 2% [1] as mentioned above. Finally, a VFM subroutine was used to extract the stiffness parameters from the simulated DIC results. The entire procedure described above was programmed using MATLAB®.

An error function C_1 has been introduced to evaluate the overall systematic error of the VFM identification. By minimizing this error function, the best test configuration can be identified. The error function C_1 is defined as:

$$C_1(\alpha,\theta) = \frac{1}{4}\sum_{ij}\left(\frac{\left|Q_{ij} - Q_{ijref}\right|}{Q_{ijref}}\right) \tag{29}$$

where α is the loading angle, θ is the off-axis angle of the material principal direction, Q_{ijref} are the reference values of the four identified material stiffness parameters input into the FE model, and Q_{ij} are the identified parameters from the simulated DIC measurements. This function represents an average identification bias over the four stiffness components. The research reported in Chapter 4 indicated that missing data on the upper and bottom free edges of the specimen have a significant influence on the identified results due to the formulation of the Virtual Fields Method. A way to deal with this would be to reconstruct the missing data the same as was done with the areas S_1 and S_3 discussed in Chapter 4 (see Figure 17). Missing data on the free edges will systematically be reconstructed the remainder of this chapter by copying the nearest data points to the missing data positions (padding). This was shown to be a very simple and efficient route to mitigating this issue.

The plots of the error function C_1 before and after the reconstruction are presented in Figure 22. As can be observed from Figure 22, the reconstruction of the data at the edges significantly reduces the error for all test parameters. In the remainder of this chapter, DIC data will systematically be reconstructed at the edges. When the off-axis angle θ is equal to 0° or 90° the identification errors are relatively large regardless of the value of the loading angle α. This can be expected because the MAF test jig only introduces tensile loading, shear loading or a combination of tensile and shear loading. With the off-axis angle near zero, the transverse stress/strain components are too small to enable stable identification of the

transverse stiffness component. The good performance of the off-axis tensile test configuration (θ=90°) confirms what has been found previously using the FE strain fields. When comparing the identification procedures using either the strains directly derived from the FE model or the strains from the DIC simulation (Figure 23), it is clear that the latter produces much larger errors than the former. This is not surprising as the error generated by the DIC process is taken into account here, which provides a much more realistic evaluation of the identification error. It can also be seen that the plot in Figure 23(a) discriminates much better between "good" and "bad" test configurations. This observation justifies the current approach, showing that simplistic procedures based on FE strains do not produce results that are sufficiently realistic. Finally, comparing Figures 22(b) and 23(a), it is observed that increased smoothing significantly affects the resulting identification error, particularly in the low angles where bending is predominant and large strain concentrations are present at the specimen corners. Nevertheless, choosing the parameters θ=90° and α=25° lead to minimal error with little effect of the increase of smoothing.

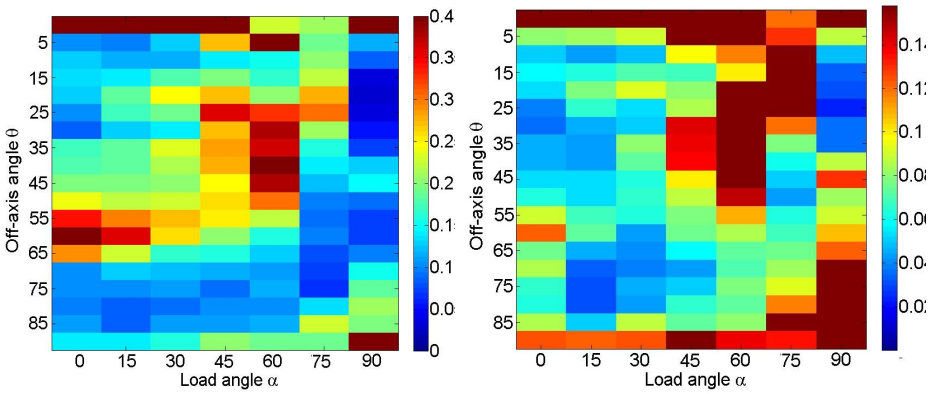

Figure 22: *Error function C_1 before (a) and after (b) reconstructing missing data at the edges (using simulated DIC strain fields with subset 30 and Gaussian smoothing kernel size of 2).*

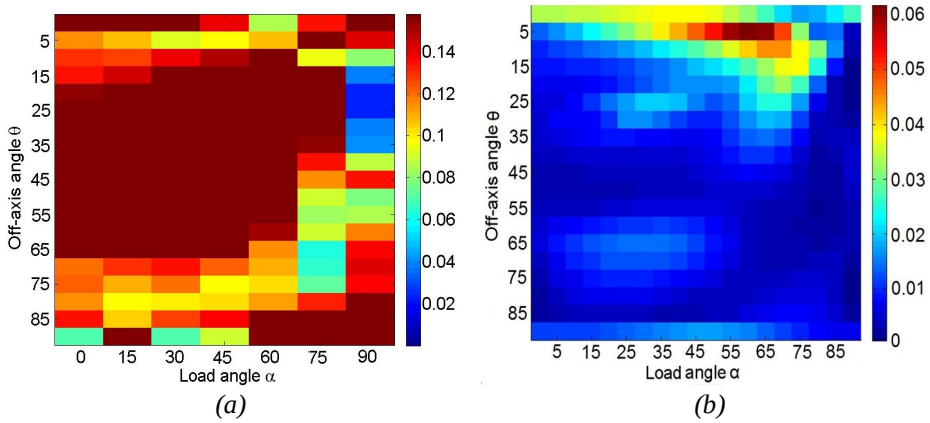

(a) *(b)*

Figure 23: *Error function C_1 from (a) DIC strain fields with subset 30 and Gaussian smoothing kernel size of 10 and (b) FE strains*

It is observed from Figures 22 and 23 that several test configurations display very high identification errors. In order to investigate the cause of this phenomenon, the strain components of one of these test configurations (θ=5° and α=60°) have been compared with the strain components of the optimal test configuration (defined by θ=25° and α=90°). It was found that the optimal test configuration exhibited lower strain gradients, especially for the strain components along the transverse direction as can be seen in Figure 24. For the test configuration with the highest identification errors (θ=5° and α=60° - Figure 24 (a)), strain values above 0.4% only occur at the corners of the specimen while most of the field of view exhibits very low strains.

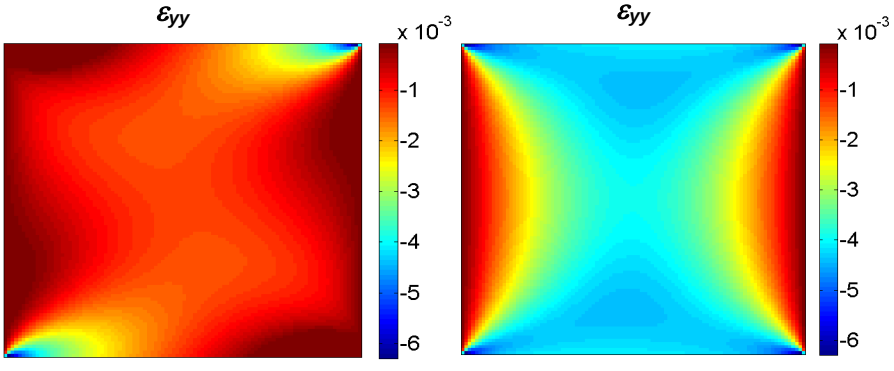

(a) *(b)*

Figure 24: *FE ε_{yy} strains for (a) θ=5° and α=60°; (b) θ=25° and α=90°.*

During the DIC process, large concentrated strains are significantly underestimated which in turn leads to a large bias in the VFM identification. This is demonstrated in Figure 25 from which a significant difference between the FE simulated strain maps and the simulated DIC strain maps can be observed. This finding shows that the systematic error originating from the low-pass spatial filtering effect of the DIC process has an important impact on the accuracy of the VFM identification. The optimal selection of the parameters of the DIC measurements (subset size, smoothing kernel) will be investigated later. In this study, the aim was to identify the best test configuration which leads to the minimum sensitivity to this systematic error.

As illustrated by the C_1 contour maps (see Figures 22 and 23), the most stable and accurate identifications are found in the tensile test configuration region (α=90°) with off-axis angles ranging between 10° and 35°. In the actual experiments, it is difficult to control the off-axis angle θ accurately so the optimized test configuration for this study was selected to be θ=25° and α=90° which is close to the centre of the favourable region to ensure accuracy of the identified results. Figure 23(a) shows the C_1 contour maps with a larger Gaussian kernel size of 10. By comparing the minima with the result in Figure 22(b) with less smoothing, it can be noted that the optimal configurations are found in the same region of the search space. In addition, this test configuration confirms the results from the previous study using FE strains in Chapter 4 (shown in Figure 23(b)), even though another good potential candidate at (θ=35° and α=30°) was found in that study, which is clearly discarded with the present approach. The current study also provides a much more realistic evaluation of the expected identification error. As can be observed from Figures 22(b) and 23(a), the level of predicted error on the identification is increased from 0.01 to 0.06 by including the DIC simulation.

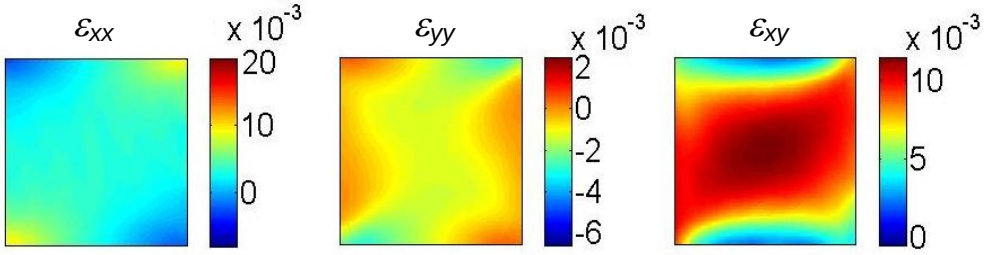

(a)

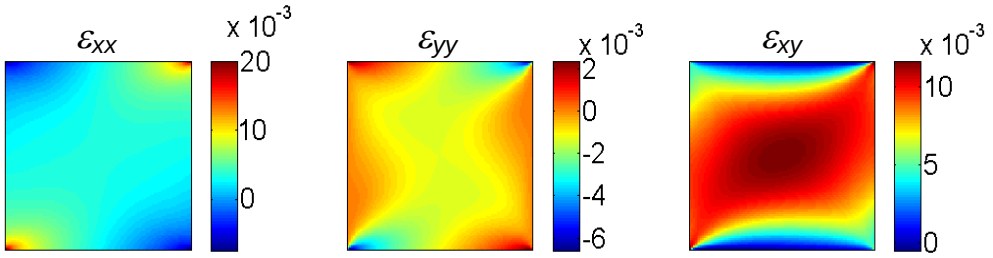

(b)

Figure 25: *(a) Strain maps from simulated DIC using synthetic images without noise (subset 30, Gaussian smoothing kernel size of 10, θ=5° and α=60°); (b) Strain maps from FE model (θ=5° and α=60°).*

The error functions corresponding to each of the identified material stiffness parameters Q_{11}, Q_{12}, Q_{22} and Q_{66} are plotted separately in Figure 26. The results shown in Figure 26 indicate that the systematic error is the largest for Q_{22} and Q_{12}. This was expected as transverse strains tend to concentrate near the corners of the specimen for most test specimen configurations. The identification accuracy of the Q_{11} and Q_{22} parameters mainly depends on the off-axis angle of the specimens. When the loading direction α is aligned with the stiffness component direction (θ=0° for Q_{11} and θ=90° for Q_{22}), the best identification of these two components is obtained. The off-axis tensile test configuration provides balanced identification of the four stiffness components.

Besides the systemic error caused by the DIC process, another important identification bias can be introduced by the through-thickness stress and strain heterogeneity which is neglected when using the plane stress assumption in the VFM routine (namely when volume integrals are approximated by the thickness multiplied by a surface integral in the principle of virtual work).

To check for this, a full 3D FE model was built up and the surface displacements from this model were input into the identification simulator. The optimized test configuration (θ=25° and α=90°) from the above systematic error study was used in this model. The identified parameters are compared with the results using 2D FE model so that the error related to this through-thickness heterogeneity can be isolated, as the 2D FE model results already capture the DIC-based errors.

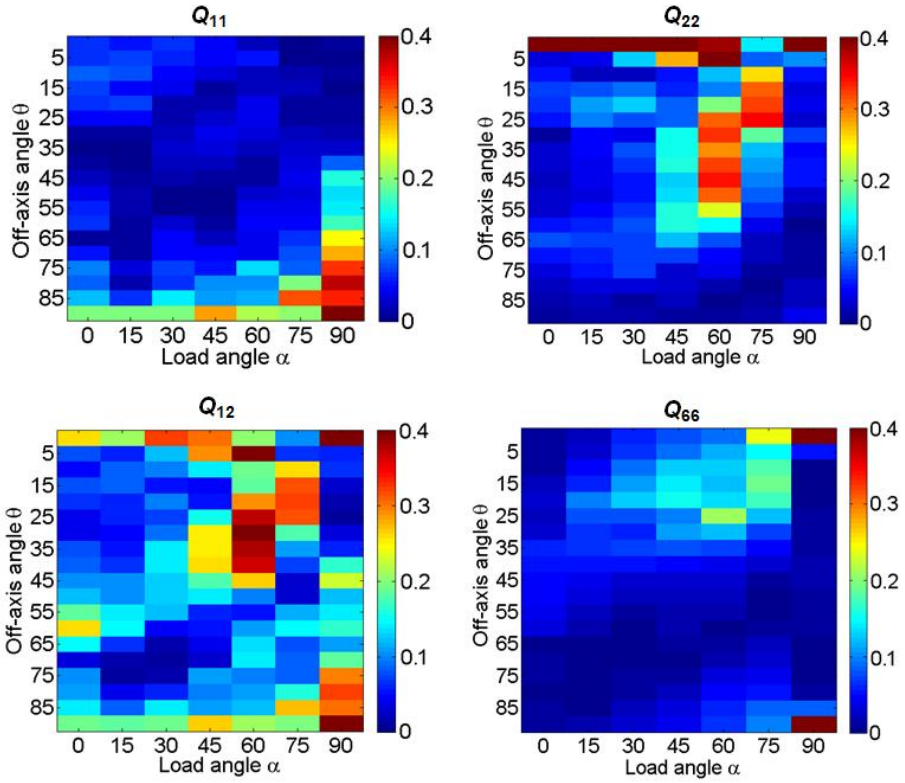

Figure 26: *Relative error for each of the identified material parameters (Q_{11}, Q_{12}, Q_{22} and Q_{66}) after reconstructing the missing data on the edges of the specimen, subset 30, Gaussian smoothing kernel size of 10.*

The identification biases are listed in Table 9. It can be seen that although the thickness of the specimen is only a fourth of its in-plane dimensions, there is still a slight over-estimation of the identification parameters. By further reducing the thickness, this identification bias can be decreased. However, a much thinner specimen would be easily damaged during the mounting of the specimen in the fixture. So it is more practical to keep this specimen thickness and correct for this bias.

Table 9: *Identification bias due to through-thickness strain heterogeneities.*

	Q_{11}	Q_{22}	Q_{12}	Q_{66}
3D FE model	148.4	67.8	29.4	31.8
2D FE model	146.3	66.2	28.2	31.1
Identification bias	1.4%	2.4%	4.2%	2.3%
DIC systematic bias	2.1%	4.6%	7.2%	2.7%

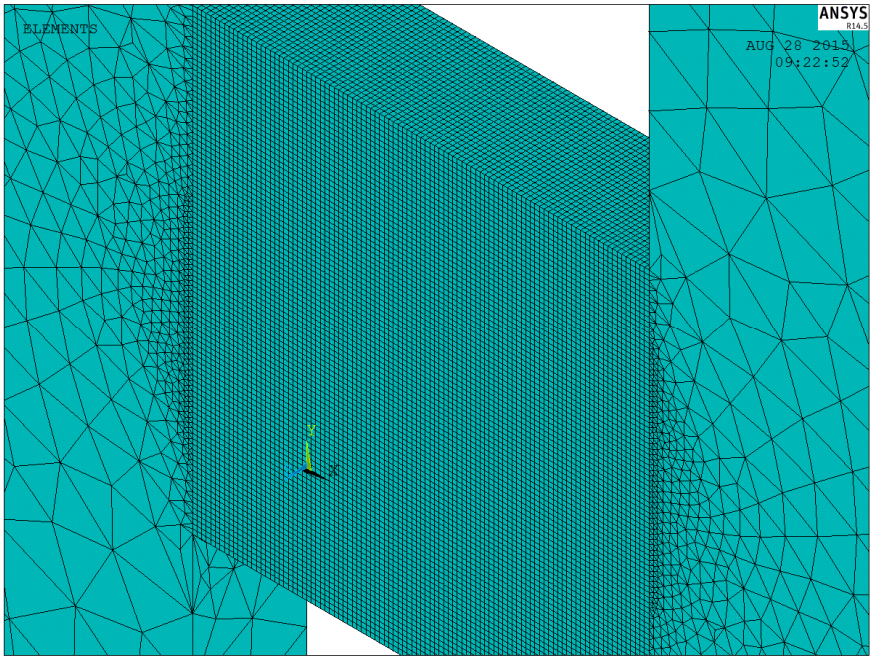

Figure 27: *3D FE model of the modified Arcan test.*

5.4 Test optimization based on the random error

Besides the systematic error, intrinsic noise of the acquired images can be propagated through the DIC and VFM processes and causes a large scattering of the identified results, especially if the signal to noise ratio is low. The noise level from actual measurements is evaluated by capturing two stationary images and then calculating the standard deviation of the difference of the two images which is around 1% of the dynamic range. According to this noise level, the noise has been simulated by adding standard Gaussian white noise to the grey level values of the synthetic images. The random error of the identified parameters is quantified by the coefficients of variation of the identified stiffness distributions obtained from repeats of the identification process with different copies of the noise on the images. The coefficient of variation is defined as the ratio of the standard deviation to the mean value to produce a scaled measure of scatter regardless of the different orders of magnitude of the stiffness components. The simulations for each test configuration were repeated 20 times to evaluate the standard deviation of the identified parameters. The error function C_2 representing the average of the coefficients of variation of the four identified material parameters Q_{11}, Q_{12}, Q_{22} and Q_{66} has been defined as follows:

$$C_2(\alpha,\theta)=\frac{1}{4}\sum_{ij}\frac{std_{ij}}{Q_{ijref}},(ij=11,22,12,66) \tag{30}$$

where (as before) α is the loading angle, and θ is the off-axis angle of the material principal direction. Q_{ijref} represents the reference values of the four identified material stiffness parameters [1], and std_{ij} is the standard deviation of the identified parameters over 20 repetitions. As can be seen from the plot of the C_2 error function in Figure 28, the off-axis shear and off-axis tensile test configuration provide the most precise identification results with the lowest standard deviation. The highest scatter is observed when the pure tensile load is applied along the in-plane direction (α=90°, θ=90°). This can be expected as the test specimen has much lower stiffness along the in-plane direction (Q_{22}=63.41 MPa) compared with the through-thickness direction (Q_{11}=143.4 MPa). When the specimen is loaded along the 2-direction, the strain component in the 1-direction is very small and highly influenced by noise.

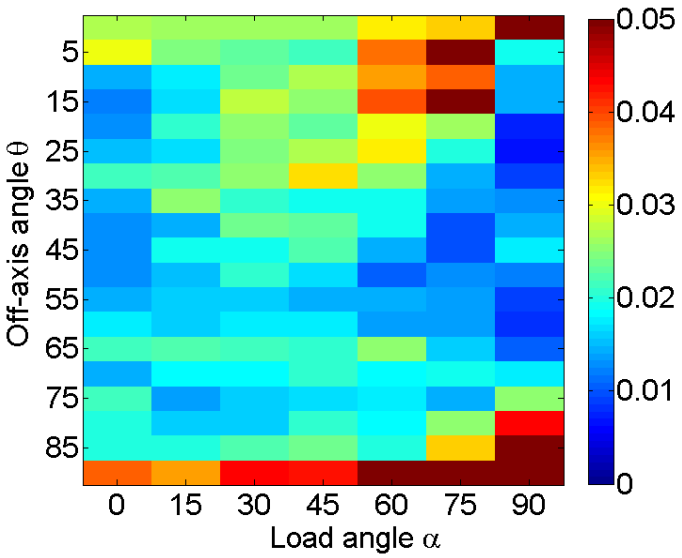

Figure 28: *Error function C_2 (average coefficient of variation) with influence of measurement noise subset 30, Gaussian smoothing kernel size of 10.*

The standard deviations of each stiffness component are plotted separately in Figure 29. For the identification of Q_{11} and Q_{22}, the lowest scatter was obtained when the loading direction is aligned with the stiffness component direction, i.e. the 1 or 2-directions, respectively, for the two stiffness parameters. The identification of Q_{66} is the most stable. The reason for this is the relatively low value of this stiffness component (Q_{66}=30.12 MPa) which results in relatively larger strain values which are less affected by noise. This confirms that balanced strain components with relatively large magnitudes can reduce both systematic and random errors. When this is combined with the previous findings in the study of the systematic error, the optimal test configuration is confirmed to be the off-axis tensile test defined by α=90° and θ=25°. This test can be referred to as the 'Short Off-Axis Tension' test (SOAT test) and is potentially an excellent candidate to become a new standard test for orthotropic materials, including fibre composites, as it can be performed in a standard test machine. This will be investigated in the forthcoming section.

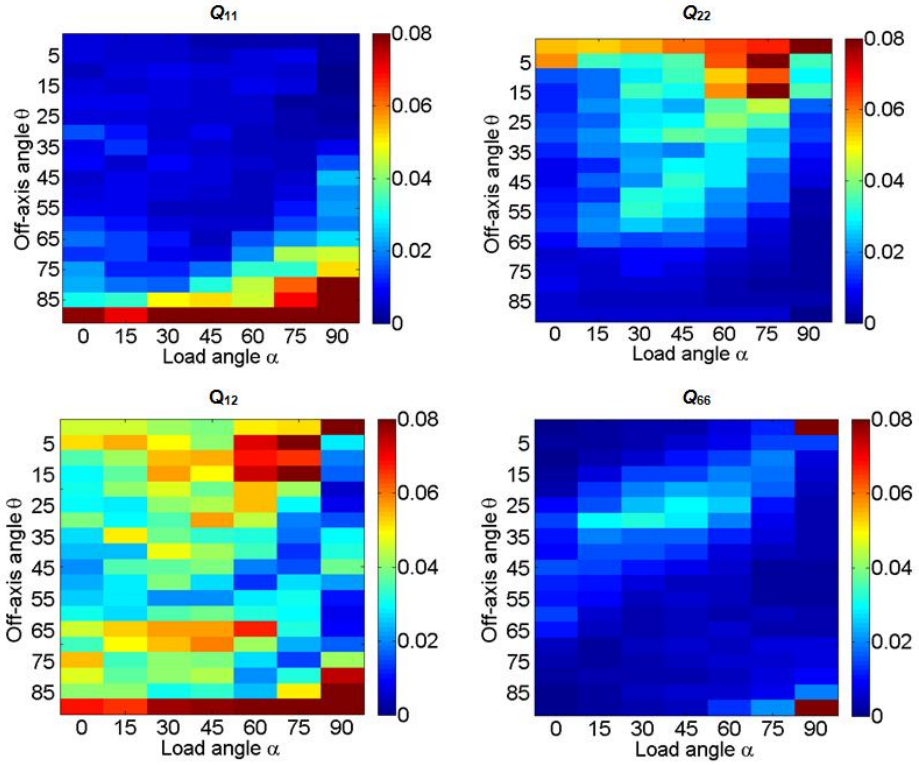

Figure 29: *Coefficients of variation of the identified results over 20 repetitions, subset 30, Gaussian smoothing kernel size of 10.*

Besides evaluating the standard deviation, the mean value of each identified parameter over 20 repetitions was also calculated. From this the identification error function C_1 can be recalculated as in eq. (31) with the mean of the distribution. For the sake of clarity, this cost function has been named C_3, and is defined as follows:

$$C_3(\alpha,\theta) = \frac{1}{4}\sum_{ij}\left(\frac{\left|\overline{Q}_{ij} - Q_{ijref}\right|}{Q_{ijref}}\right), (ij = 11,22,12,66) \tag{31}$$

where $\overline{Q}_{ij}$ is the mean value of 20 repetitions, Q_{ijref} are the reference values of the four identified material stiffness parameters [1] input into the FE model, and (as before) α is the loading angle, and θ is the off-axis angle of the material principal directions. The results are plotted in Figure 30, from which it is observed that the contour map nearly coincides with the plot of the systematic error in Figure 22(b). This shows that the noise does not produce a significant additional bias.

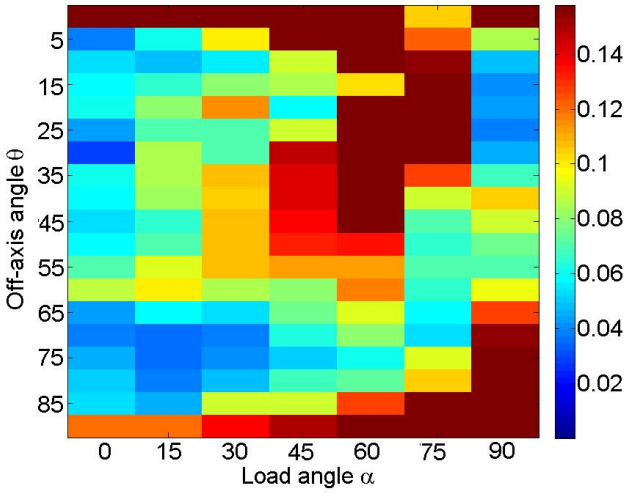

Figure 30: *Error function C_3 (mean value of identified results over 20 repetitions), subset 30, Gaussian smoothing kernel size of 2.*

5.5 Selection of subset sizes and smoothing levels

As was demonstrated before, the DIC process hidden inside most of the commercial DIC software strongly influences the quality of the measured strain maps and can lead to a significant bias on the VFM identification. It is therefore important to systematically study the effect of the main DIC parameters (subset size, smoothing kernel) and define optimal values for these. This enables a more rational approach to these important choices which directly impact the quality of the results. In accordance with the results from the study of the systematic and the random errors in the previous sections, the 'Short Off-Axis Tension' (SOAT) test configuration (θ=25°, α=90°) has been selected as the most optimal for conducting the physical experiments. Based on this most optimal test configuration, two main DIC process parameters (subset size, smoothing kernel) were chosen here as variables to study the optimal combination of these two parameters. Subset size is the main parameters in DIC process and is critical to the accuracy of the measurement results. However, the most of users of the existing DIC techniques still rely on experience and intuition to manually define the size of the subset. Spatial smoothing of the displacements is also necessary to improve the strain resolution, particularly in the low elastic strain range considered here. However, while reducing the random component of the error, smoothing can significantly increase the systematic part of the error as was shown earlier in this thesis. At a certain stage, the systematic error overtakes the random error, so there is an optimal point or trade off between the two. Therefore, the optimal choice of the two DIC process parameters (subset size,

smoothing levels) will be investigated by seeking for the minimal overall identification error of systematic and random error together. In this study, the smoothing technique is Gaussian smoothing of the strain maps. Other types of smoothing could have been investigated but it is hypothesized that the regularization parameter (kernel size here) is more important than the actual smoothing technique used, as they all provide some form of low pass filtering where the cut-off frequency is driven by the regularization parameter. The identification errors will be obtained by comparing the identified values with the reference values (Q_{11}=143.4 MPa, Q_{22}=63.41 MPa, Q_{12}=26.01 MPa, Q_{66}=30.12 MPa) from previous chapters. A way to define the optimal point (minimal error) is to consider a 95% confidence interval, which is the mean plus or minus twice the standard deviation. Therefore, the largest possible error, with a 95% confidence, is obtained as follows: if the mean is below the reference, it will be the mean minus twice the standard deviation; if the mean is above the reference, then it will be the mean plus twice the standard deviation. By plotting this maximum error, the optimal parameters and a confidence interval are identified. The error function is below where the variables used are the subset and kernel sizes:

$$C_4(sub,\ker) = \frac{1}{4}\sum_{ij}\left(\frac{\max\left|Q_{ij}^{C} - Q_{ijref}\right|}{Q_{ijref}}\right), (ij = 11,22,12,66) \tag{32}$$

where Q_{ijref} are the reference values of the four material stiffness parameters [2] input into the FE model, Q_{ij}^{C} are the stiffness parameters with 95% confidence interval which is defined as follows:

$$Q_{ij}^{C}(sub,\ker) = \overline{Q}_{ij} \pm 2std_{ij}, (ij = 11,22,12,66) \tag{33}$$

Where $\overline{Q}_{ij}$ is the mean of the four stiffness parameters over 20 repetitions calculated with different subset and kernel sizes, and std_{ij} is the standard deviation of the four stiffness parameters over 20 repetitions.

First, it is possible to evaluate the systematic part of the error by evaluating C_4 without any noise. This leads to the systematic error displayed in Figure 31. As expected, this error increases for increasing subset sizes and smoothing levels. Then, adding noise, it is possible to evaluate the random part of the error by subtracting the systematic error from the total error obtained from C_4 with noise. This part of the error increases moderately with decreasing subset size, and decreases more sharply with increasing smoothing levels. At some stage, these two curves cross over, showing that there should be an optimum trade-off point between the two types of error. This optimum is clearly seen on Figure 32 which shows that a kernel size equal to 11 and a subset size of 40x40 provides minimum value of C_4.

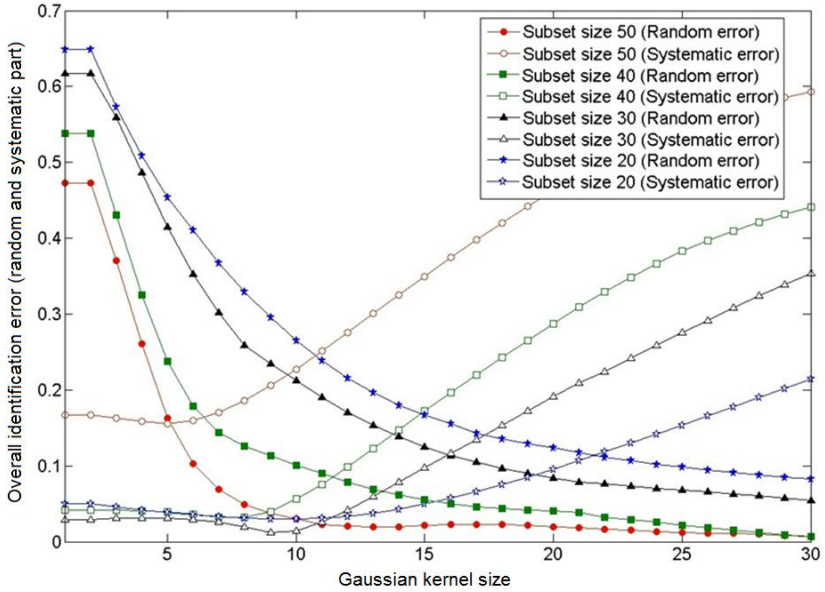

Figure 31: *Systematic and random errors*

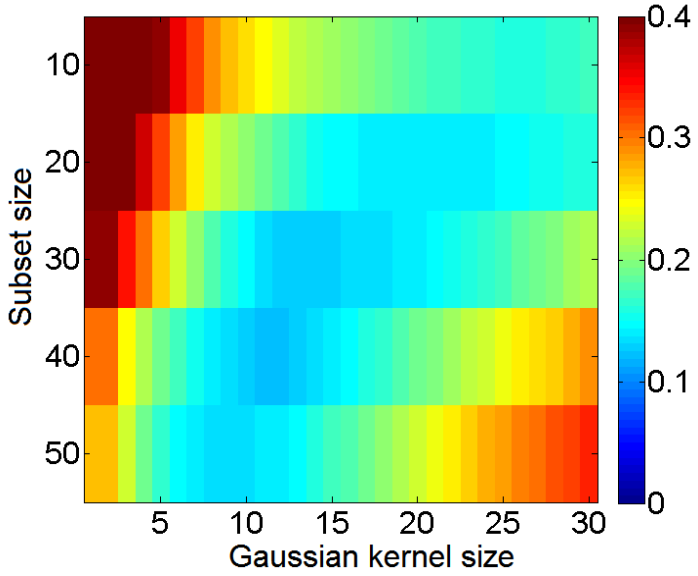

Figure 32: *Error function C_4 with different subsets and Gaussian smoothing kernel sizes*

5.6 Confidence interval and effect of image averaging

After obtaining the systematic and random errors predicted from the above study, confidence intervals (CI) can be calculated to indicate the reliability of the identification. The confidence interval of each identified stiffness parameter is defined as follows corresponding to a 95% confidence level:

$$CI_{ij}=Q_{ij}\,(\textit{without noise})\pm 2std_{ij}\,(\textit{standard deviation with noise}),\quad (ij=11,22,12,66) \tag{34}$$

As was observed in section 5.4, the averaging of each identified parameter over 20 repetitions will reduce the random error and leave only the systemic error. This finding indicates that the averaging of multiple static images may provide an efficient way to reduce the data dispersions caused by image noise. In a practical/physical testing context when the specimen is loaded up to a certain level and stabilized, it is possible to record many images and then average them to filter out camera noise. The effect of image averaging has been further investigated using the simulated DIC experimental procedure developed in this Chapter. The test configuration and other DIC test parameters were determined from the above optimization study. The confidence intervals of the four stiffness parameters have been calculated individually based on averaging different numbers of images (5, 10, 20, 50, and 100). The results are plotted in Figure 33, where the black dots show the upper limits of the confidence interval and the red dots represent the lower limits.

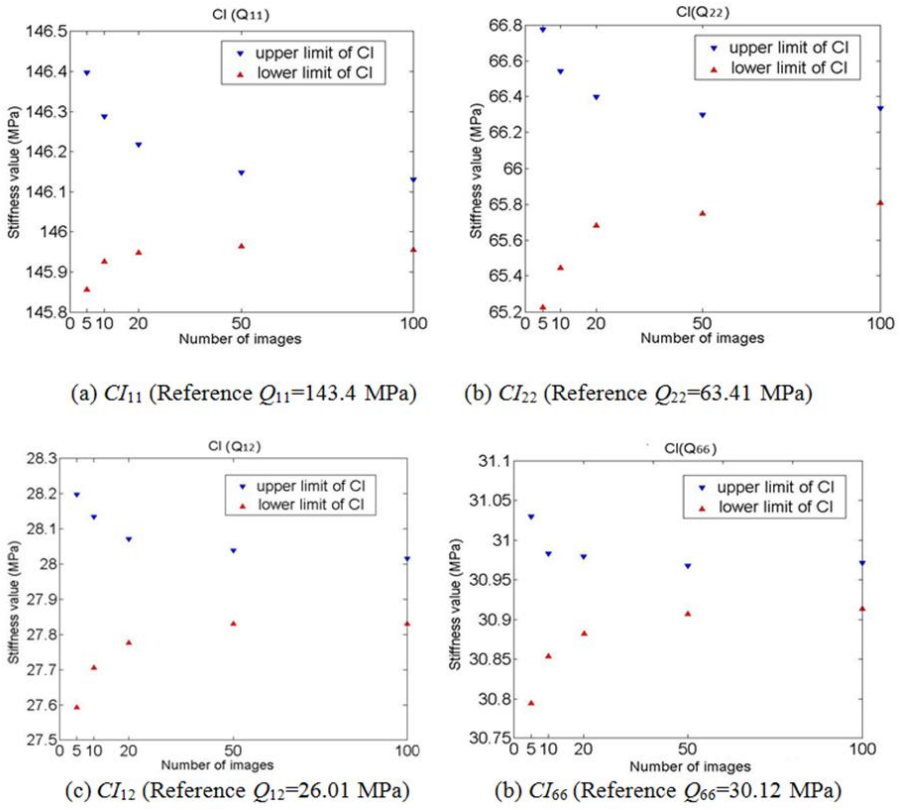

Figure 33: *Confidence intervals (CIs) of the four stiffness parameters.*

As expected, it is seen from Figure 33 that the confidence intervals reduce when the number of images is increased. This phenomenon demonstrates that the averaging of multiple stabilized images exerts an influence on the identification. Thus, by utilising this procedure instead of increasing the smoothing level, the random error can be effectively reduced without raising the systematic bias. Furthermore, the results also indicate that the elastic stiffness parameters tend to converge to values that are slightly larger than the reference values. This is due to the systematic error originating from the low pass filtering effect of the DIC process. Although the random error of the measurement is significantly reduced, the systematic bias still exists and results in an over-prediction of the stiffness parameters. When the number of images exceeds 50, the confidence interval stabilizes, and the optimal number of images was therefore set to 50.

5.7 Final experimental validation using all the optimal test parameters

The Short Off-Axis Tensile (SOAT) experiments (see Figure 34) were conducted on using 3 different but identical specimens to validate the findings from the optimization investigation. The testing was set up according to the optimized test parameters selected from the numerical study. The stiffness parameters were calculated by averaging the DIC measured displacement results from two back-to-back cameras firstly and perform the VFM identification using this averaging displacement fields. Subset size and smoothing kernels were selected to be 40 and 10 according to the systematic and random error study previously reported. The detailed performance of this setup is given in Table 10.

The resolutions reported in Table 10 were evaluated as the standard deviation of the displacement and strain maps of two consecutive images of the stationary specimen. In order to validate the effect of image averaging investigated in Section 5.6, the experiments were conducted by capturing single and multiple images of the stabilized specimens. All the specimens were load up to only 100 N to ensure that the deformations were not beyond the range of linear elasticity. After around 30 s when the specimen has stabilized (stable force reading), multiple images were captured with the rate of one image per second. This measurement procedure was then repeated 20 times on the same day and the specimen was kept in the fixture/machine during the process. Both the mean value and the standard deviation of the identified material stiffness parameters were then calculated, and the results were subsequently compared with both the simulated data and the reference experimental data. The simulation data was calculated using the simulated DIC measurement procedure and based on the same realistic/physical images captured in this experiment. The reference values for the elastic properties were obtained using ASTM standard tests in [7], as well as from measurements conducted using the modified MAF test jig with tensile tests along the in-plane and through-thickness directions and shear tests using butterfly-shaped specimens [1]. The reference values reported in [7] and [1] are very similar.

Table 10: *Experimental DIC settings and performances (MatchID DIC package).*

Technique Used	2D image correlation
Subset size	40 x 40 pixel^2
Shift	20 pixel (50%)
Shape function	Affine
Interpolation function	Bicubic polynomial
Correlation criterion	Approximated Normalized Sum of Squared Difference (Approximated NSSD)
Presmoothing applied to the images	None
Camera	8 bit, 2048 x 2048 pixel^2
Field of view	24mm x 24mm
Displacement field:	
Resolution	0.2 μm / 0.017 pixel
Strain field:	
Differentiation method	Finite differences
Smoothing method	Gaussian smoothing (kernel size 11)
Resolution	1.3x10^{-4}

Figure 34: *Short Off-Axis Tensile (SOAT) test experimental set up.*

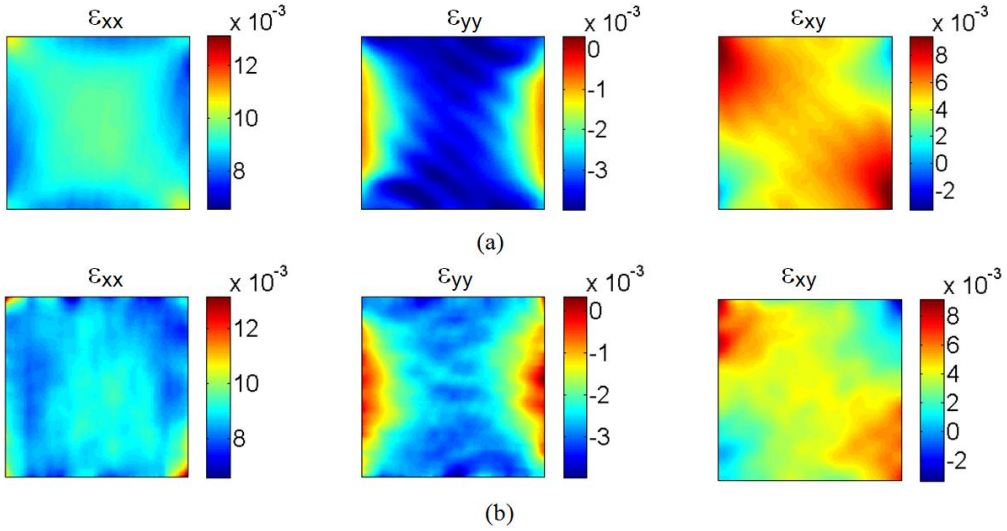

Figure 35: *(a) Strain maps from DIC simulations (subset 40x40, smooth kernel 11, load 100 N); (b) Strain maps from physical experiments (the average of two back-to back cameras, subset 40x40, smooth kernel 11, load 100 N)*

Figure 35 displays the comparison of the two sets of strain maps obtained from the simulated DIC experiments and the physical measurements. It can be observed that the DIC simulator provides a good prediction of the strain maps obtained from the physical measurements. The mean values of the identified stiffness components obtained over 20 repetitions using 50 averaged images are listed in Table 11 below.

Table 11: *The mean value from 20 repetitions using 50 average images.*

	Q_{11} [MPa]	Q_{22} [MPa]	Q_{12} [MPa]	Q_{66} [MPa]
Specimen 1	149.3	68.1	27.9	32.9
Specimen 2	147.6	70.8	29.6	31.1
Specimen 3	150.1	69.1	29.9	32.4
Mean value	149.0	69.3	29.1	32.1
DIC Simulation	146.1	66.0	27.9	30.9
Reference data [1]	143.4	63.4	26.0	30.1

The experimental identified parameters have a good correlation between the simulation results. Both the experimental and the simulated results display an over-prediction of the stiffness parameters compared with the reference data. This is mainly due to that the DIC process smooths out of local strain peaks and creates the systematic error. The material parameters identified from the physical experiments display slightly larger mean values than that predicted using the simulated DIC procedure. This is not surprising as other sources of error come into play like non-uniform lighting or lens distortions [39]. Tables 12 and 13 provide the standard deviations and coefficients of variation of the identified results over 20 repetitions using either the average of 50 images or a single image. The results using the average of 50 images display a significant reduction of the standard deviation of the 20 repeated measurements. This confirms the findings from the simulation study in section 5.6. However, the efficiency of this method in the experiments is not as significant as was suggested by the results of the numerical study, and the resulting standard deviation has not come down to the expected value.

Table 12: *The standard deviation and coefficients of variation from 20 repetitions using 50 averaged images.*

	Q_{11} [MPa]	Q_{22} [MPa]	Q_{12} [MPa]	Q_{66} [MPa]
Specimen 1	0.169	0.646	0.225	0.132
Specimen 2	0.155	0.623	0.203	0.133
Specimen 3	0.223	0.715	0.250	0.159
Mean value	0.182	0.661	0.226	0.131
DIC Simulation	0.0458	0.138	0.0520	0.0152
Coefficients of variation				
Experimental	0.12%	0.95%	0.78%	0.41%
DIC simulation	0.030%	0.20%	0.18%	0.047%

Table 13: The standard deviation and coefficients of variation from 20 repetitions using one single image.

	Q_{11} [MPa]	Q_{22} [MPa]	Q_{12} [MPa]	Q_{66} [MPa]
Specimen 1	0.345	1.42	0.302	0.251
Specimen 2	0.389	1.39	0.295	0.230
Specimen 3	0.413	1.62	0.337	0.278
Mean value	0.382	1.48	0.311	0.253
DIC Simulation	0.275	0.993	0.205	0.122
Coefficients of variation				
Experimental	0.25%	2.1%	1.07%	0.79%
DIC simulation	0.18%	1.5%	0.73%	0.39%

In order to further investigate the cause of this deviation, the difference of the grey level intensity between two consecutive images is compared with the average of different numbers of images. The evolution of the noise level by averaging different numbers of stabilized images is illustrated in Figure 36.

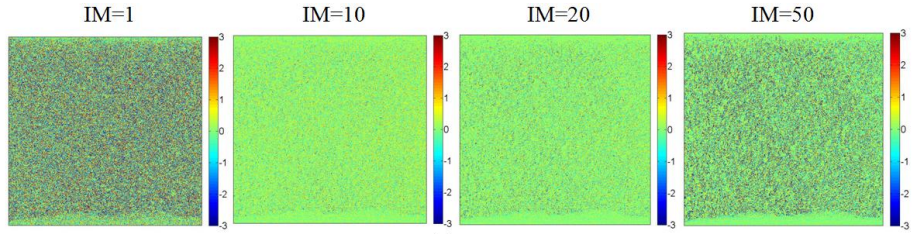

(a)

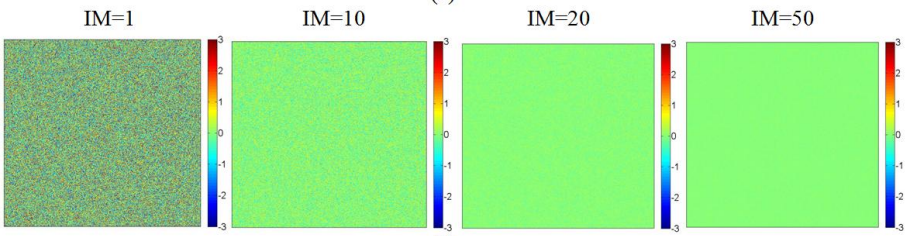

(b)

Figure 36: *The noise level (in grey level values) of the images using either a single image (IM=1) or the average of multiple images: (a) based on the results of the physical experiments; (b) based on simulation.*

The previous simulation study in section 5.6 demonstrated that the noise effect is gradually reduced when the number of images that are used in the averaging is increased (shown in Figure 33). However, by evaluating the images from the physical measurements (shown in Figure 36(a)), the situation is not quite the same as that observed from the predictions of the simulated experiments. It can be seen that when taking up to 10 images and averaging them, the noise influence is reduced as in the numerical prediction. However, by taking images continuously up to 50 the noise is seen to increase again. This is the reason why the standard deviation of the experimental results is not significantly reduced using the optimal number of images (50). This likely cause of this phenomenon is that the specimen was not experiencing static steady state conditions when the recording of the multiple images was conducted. Since the integration time was one second per image, this indicates that the patterns on the surface of the specimen may have displayed a slight variation after 10 seconds. A likely explanation for this time-dependency problem is that the PVC foam material displays viscoelastic behaviour, hence creep can occur over 50 seconds even when the load appears to be stabilized. Other effects like changes of lighting conditions or air movements can also play a role. Furthermore, camera heating is also an important aspect. A way to resolve this issue would be to increase the rate of image acquisition to reach the optimal number of images within 10 seconds. For the current study, 10 images are used as the optimal image number instead of 50. Table 14 displays the standard deviation calculated using 10 instead of 50 images. Comparing with the data in Table 12, the difference between the test results and the predicted standard deviation from DIC simulation is significantly reduced.

Table 14: The standard deviation from 20 repetitions using 10 averaged images.

	Q_{11} [MPa]	Q_{22} [MPa]	Q_{12} [MPa]	Q_{66} [MPa]
Specimen 1	0.118	0.403	0.138	0.0689
Specimen 2	0.095	0.363	0.117	0.0534
Specimen 3	0.132	0.471	0.152	0.0692
DIC Simulation	0.0701	0.235	0.0914	0.0376

6. Conclusions

This PhD dissertation presents work that has focused on the establishment of an efficient and reliable methodology for simultaneous identification of the orthotropic stiffness components of polymer foam in one single test. The aim has been to develop a robust optimization procedure to predict the uncertainty of the experimental characterisation of polymer orthotropic foam materials and to optimize the design of the experiments. However, the developed methodology is generic, and as such it will in principle be applicable to other material systems.

In the first part of the study, the basic framework with the combination of DIC and an extraction VFM routine has been developed. The preliminary experimental investigation shows that the accuracy of the identification of the elastic stiffness coefficients heavily depends on the test configuration as well as on the full-field measurement parameters such as camera noise, spatial resolution and smoothing levels. Therefore, the most feasible and efficient way to solve this problem is to modify the test configuration so that more transverse stresses/strains are introduced thus reducing the effect of noise.

Based on the preliminary study, a modified Arcan test fixture (MAF) was used for the testing, and an optimization routine based on finite element simulated strain fields was developed to identify the best test configuration as a function of loading angle and material principal directions. The effect of noise and missing data were included into the optimization study as the two main error sources. The experimental results validated the findings of the numerical optimization study in that the off-axis tensile test gave an improved identification of the orthotropic stiffness components of the polymer foam considered. Missing strain data at the free edges proved to have a very significant influence on the identification results. This was accounted for by using a data extrapolation scheme which proved to be successful. The larger sensitivity of the shear test to missing data as opposed to the off-axis tensile test was also revealed in the experimental data and confirmed the numerical analysis results. This is due to large bending stresses at the free edges of the specimen. The identification results were significantly affected by the size of the virtual mesh, particularly for the parameters Q_{22} and Q_{12}. This may be caused by errors introduced by inappropriate spatial resolution of the measurements. Different Virtual Fields process the bias caused by inappropriate local spatial resolution differently, hence different stiffness values are obtained. The only way to assess this issue rigorously is to simulate the realistic/physical DIC measurement process.

In order to solve the issues discussed above, a more advanced optimization routine was developed to bring further improvements to the current procedure. Optimal test

parameters have been sought to provide a reliable identification of all the elastic stiffness parameters in one single test using DIC and VFM. The image recording from physical experiments was mimicked by deforming the reference speckle patterns using displacements derived from FE analysis. DIC and VFM routines were used to process the synthetic speckle patterns and to extract all the elastic stiffness parameters. By using this method, a large number of simulated experiments were generated efficiently with varying testing parameters. For the current study, the test parameters selected were the loading angle (α), the off-axis angle (θ) relative to the material principal direction, the subset size and the smoothing kernel. Several error functions have been defined to describe the influence of both the systematic and random errors on the VFM identified results. Based on this, an optimum test configuration was identified by minimizing the identification error.

The study of the systematic error has demonstrated that the low pass filtering effect of the DIC process can bring significant bias to the identification results. By using the simulated DIC measurements, this error source can be included into the optimization study and also provide a more realistic prediction of the expected identification error. It was further observed that the random error can be reduced by averaging over multiple images. By combining the results from the analyses of the systematic and random errors, a Short Off-Axis Tensile (SOAT) test (θ=25°, α=90°) was chosen as the optimized test configuration.

Based on the optimized test configuration, several optimal test parameters related to the DIC process were determined. The results showed that increasing the subset size and the smoothing level exerted opposite effects on the systematic and random errors of the VFM identification. It is therefore important to balance out the two different sources of error when choosing the optimal DIC processing parameters.

The confidence interval of the parameters obtained from the simulations was calculated based on the systematic and random errors. The study of image averaging revealed that the confidence intervals tend to stabilize when the number of images used in the averaging is increased, whereas the systematic error remains unchanged and causes over-prediction of the identified material parameters.

Finally, the predictions of the simulated experiments in terms of identified material parameters have been validated against physical experiments. From this it was further concluded that the simulated measurement procedure can provide a realistic quantification of the identification error, and also that the optimized testing configuration and DIC parameters led to a stable and accurate parameter identification. However, when using the average of the optimal number of images, the random error of the experimental results was not reduced as effectively as was predicted from the simulated experiments. The reason for this is hypothesized to be

the lack of stability of the imaging conditions during the image recording process. To reduce this error, a higher frame rate would be required to capture the optimal number of images within as short a time as possible.

7. Future work

The work carried during this PhD project has included extensive modelling, experimental validation and optimization studies. The final methodology proposed has been proven to be able to provide reliable and accurate identification of elastic constitutive parameters. However, some of the issues addressed in this work require further investigation. One such issue is the visco-elastic (creep) behaviour displayed by the polymer foam considered (cross-linked PVC foam) during the final experimental study of the effect of image averaging. Thus, it would be interesting to increase the rate of image acquisition to further investigate the optimal number of images which can provide the lowest random error.

Another important research direction is to study additional error sources that were not considered in the present work, for instance slight misalignments between the specimen surface and the camera sensors, non-uniform lighting and light noise from the environment, the shape functions or the interpolation functions hidden in DIC commercial package, and also the fact that the speckle pattern is often produced in a non-optimized and non-reproducible manner with paint spray. A follow-up on this work will be to include such errors and perform a sensitivity analysis. The long term objective would be to develop a new generation of robust and reliable test methods which can be used in industry in the future. To reach this goal, extensive optimization investigations of all relevant test parameters should be conducted.

The work presented in this PhD dissertation represents a step towards the development of new standard tests based on full-field measurements and inverse identification, which will enable faster and more cost-effective materials testing in the future. There are still a few steps in this left to investigate, develop and validate before this is achieved, but the end goal appears to be within reach. A key issue is the systematic error, but it is likely that this will soon be mitigated due to technological development and the availability of affordable high quality, high spatial resolution (16 Mpixels) and low noise (sCMOS) cameras. The last step is to make all the elements of this procedure robust to routine use by non-experts.

Finally, materials with more complex material properties, for instance heterogeneous materials, can be investigated to test the current experimental methodology. The formulation of the VFM described in Chapter 2 needs to be adjusted for heterogeneous materials. This can be done by modelling the spatial evolution of the constitutive parameters with a suitable function of the spatial coordinates. Some preliminary study has been done during this project using FE modelling to simulate a specimen with a polynomial spatial distribution of the material elastic parameters. Based on the simulated FE strain fields, the VFM routine can successfully extract all the coefficients of this polynomial. However, the scope of this project has been to apply the developed methodology on experimental validation for industrially practical/physical foam material systems. Due to limitations of the manufacturing processes, it is extremely difficult to produce polymer foam core materials which have a regular spatial distribution, and also to

suggest reasonable guesses for the polynomials used to describe the constitutive parameters to construct the virtual fields. Therefore, further experimental study should be conducted to investigate suitable material systems which can be used to validate the possibility of this possible future application of the methodology.

Bibliography

[1] Landis F, Schenker O, Tovar Reaños MA, Vonnahme C, Zitzelsberger S (2012) An Overview on Current Climate Policies in the European Union and its Member States.

[2] Taher ST, Thomsen OT, Dulieu-Barton JM, Zhang S (2011) Determination of mechanical properties of PVC foam using a modified Arcan fixture. Composites Part A: Applied Science and Manufacturing., 43(10), 1698-1708

[3] Taher ST, Thomsen OT, Dulieu-Barton JM (2011) Bidirectional Thermo-Mechanical Properties of Foam Core Materials Using DIC. Thermomechanics and Infra-Red Imaging., 7, 67-7418

[4] Gdoutos EE, Daniel IM, Wang KA (2001) Multiaxial characterization and modeling of a PVC cellular foam. J. Thermoplast. Compos. Mater., 14(5), 365–373

[5] Kanny K, Mahfuz H, Thomas T, Jeelani S (2004) Static and dynamic characterization of polymer foams under shear loads. J. Compos. Mater., 38(8), 629–639

[6] Kabir ME, Saha MC, Jeelani S (2006) Tensile and fracture behavior of polymer foams. Mater. Sci. Eng., A, 429(1–2), 225-235

[7] Daniel I, Cho JM (2011) Characterization of Anisotropic Polymeric Foam under Static and Dynamic Loading. Exp. Mech., 51(8), 1395-1403

[8] Zhang S, Dulieu-Barton JM, Fruehmann R, Thomsen OT (2012) A Methodology for Obtaining Material Properties of Polymeric Foam at Elevated Temperatures. Exp. Mech., 52 (1), 3-15

[9] DIAB (2011) Divinycell PVC datasheet. http://www.diabgroup.com

[10] Sutton MA, Bruck HA, Chae TL, Turner JL (1990) Development of a computer vision methodology for the analysis of surface deformations in magnified images. ASTM STP-1094; MICON-90. Advances in video technology for micro-structural evaluation of materials, 109–134.

[11] Sutton MA, Yan J, Avril S, Pierron F, Adeeb S (2008) Identification of heterogeneous constitutive parameters in a welded specimen: uniform stress and virtual fields methods for material property estimation. Exp. Mech., 48 (4), 451-464

[12] Bruno L, Poggialini A (2005) Elastic characterization of anisotropic materials by speckle interferometry. J. Appl.Mech., 45, 205–212.

[13] Surrel Y (1994) Moire´ and grid methods: a signal processing approach. In: Interferometry ’94: Photomechanics. Vol. 2342 (J. Pryputniewicz and R. J. et

Stupnicki, Eds). The International Society for Optical Engineering, SPIE, Bellingham, WA: 213–220.

[14] Surrel Y (1996) Design of algorithms for phase measurement by the use of phase stepping. Appl. Optics 35, 51–60.

[15] Avril S, Vautrin A, Surrel Y (2004) Grid method: application to the characterization of cracks. Exp. Mech., 44, 37–43

[16] Hendricks MAN (1991) Identification of the mechanical properties of solid materials. Doctoral Dissertation, Eindhoven University of Technology, Eindhoven, The Netherlands.

[17] Geymonat G, Hild F, Pagano S (2002) Identification of elastic parameters by displacement field measurement. C. R. Acad. Sci., 330, 403–408.

[18] http://www.camfit.fr/index.php

[19] Dym CL, Shames IH (1973) Solid Mechanics: A Variational Approach. McGraw-Hill Book Co., Tokyo.

[20] Grédiac M, Pierron F, Avril S, Toussaint E (2006) The virtual fields method for extracting constitutive parameters from full-field measurements: a review. Strain: an International Journal for Experimental Mechanics. 42, 233-253.

[21] Avril S, Pierron F (2007) General framework for the identification of elastic constitutive parameters from full-field measurements. Int J Solids Struct., 44, 4978-5002.

[22] Kajberg J, Wikman B (2007) Viscoplastic parameter estimation by high strain-rate experiments and inverse modeling—speckle measurements and high-speed photography. Int J Solids Struct 44, 145–164.

[23] Kajberg J, Lindkvist G (2004) Characterisation of materials subjected to large strains by inverse modelling based on in-plane displacement fields. Int J Solids Struct 41:3439–3459.

[24] Pierron F (2010) Identification of Poisson's ratios of standard and auxetic low density polymeric foams from full-field measurements. J. Strain Anal. Eng. Des., 45(4), 233-25

[25] Pierron F, Vert G, Burguete R, Avril S, Rotinat R, Wisnom M (2007) Identification of the orthotropic elastic stiffnesses of composites with the virtual fields method: sensitivity study and experimental validation. Strain, 43(3), 250-25

[26] Rossi M, Pierron F (2012) On the use of simulated experiments in designing tests for material characterization from full-field measurements. Int. J Solids Struct., 49 (3-4), 420-435

[27] Hamilton AR, Thomsen OT, Madaleno L A.O, Jensen LR, Rauhe JC, Pyrz R (2013)
Evaluation of the Anisotropic Mechanical Properties of Reinforced PolyurethaneFoa ms. Composites Science and Technology., 87, 210-217.

[28] Chu TC, Ranson WF, Sutton MA (1985) Applications of digital-image-correlation techniques to experimental mechanics. Exp. Mech., 25 (3), 232-244.

[29]ARAMIS user manual, GOM. http://www.gom.com

[30] Moulart R, Avril S, Pierron F (2006) Identification of the through-thickness rigidities of a thick laminated composite tube. Composites Part A: Applied Science and Manufacturing., 37 (2), 326-336

[31] Robert MJ (1998) Mechanics Of Composite Materials. CRC Press. ISBN-10: 156032712X.

[32] Pierron F, Grédiac M (2012) The Virtual Fields Method. Springer New York. ISBN 978-1-4614-1823-8

[33]Toussaint E, Grédiac M, Pierron F (2006) The virtual fields method with piecewise virtual fields. Int. J. Mech. Sci., 48(3), 256-264. (doi:10.1016/ j.ijmecsci.2005.10.002)

[34] Pierron F, Vautrin A (1994) Accurate comparative determination of the in-plane shear modulus of T300/914 by the Iosipescu and 45° off-axis tests. Compos. Sci. Technol., 52 (1), 61-72

[35] Evaluation of measurement data — Guide to the expression of uncertainty in measurement, JCGM 100:2008
http://www.bipm.org/utils/common/documents/jcgm/JCGM_100_2008_E.pdf (last accessed on July 29th 2014)

[36] Rossi M, Lava P, Pierron F, Debruyne D, Sasso M (2015) Effect of DIC spatial resolution, noise and interpolation error on identification results with the VFM. Strain: an International Journal for Experimental Mechanics., in revision.

[37] MatchID – www.matchid.org (last accessed 29th July 2014)

[38] Lava P, Cooreman S, Coppieters S, Strycker MD, Debruyne D (2009) Assessment of measuring errors in DIC using deformation fields generated by plastic FEA. Opt Lasers Eng., 47, 747-753

[39] Lava P, Van Paepegem W, Coppieters S, De Baere I, Wang Y, Debruyne D (2013) Impact of lens distortions on strain measurements obtained with 2D digital image correlation. Opt Lasers Eng., 51, 576-584

Appended papers

Paper 1: Wang, Peng, Pierron, F, Thomsen, Ole Thybo (2011). Identification of Material Parameters of PVC Foams Using Digital Image Correlation and the Virtual Fields Method. Proceedings of the 18th International Conference on Composite Materials (ICCM-18). Jeju Island, Korea.

Paper 2: Wang P, Pierron F, Thomsen OT (2013). Identification of material parameters of PVC foams using Digital Image Correlation and the Virtual Fields Method. Exp. Mech. 53(6): 1001-1015

Paper 3: Wang, P., Pierron, F, Rossi, M, Lava, P, Thomsen, O.T. (2013). Optimized experimental characterisation of PVC foam using DIC test and The Virtual fields method. Proceedings of the 19th International Conference on Composite Materials (ICCM-19), Montreal, Canada.

Paper 4: Wang, P., Pierron, F., Rossi, M., Lava, P., Thomsen, O.T. (2014), Optimized experimental characterisation of polymeric foam material using DIC and the Virtual fields method . Accepted to Strain - An international Journal to Experimental Mechanics (doi: 10.1111/str.12170).

ISSN (online): 2246-1248
ISBN (online): 978-87-7112-423-1

AALBORG UNIVERSITY PRESS